Adsorption-induced deformation of nanoporous materials—A review

Gennady Y. Gor, Patrick Huber, and Noam Bernstein

Articles you may be interested in

Substrate induced changes in atomically thin 2-dimensional semiconductors: Fundamentals, engineering, and applications
Applied Physics Reviews **4**, 011301 (2017); 10.1063/1.4974072

Size effects and charge transport in metals: Quantum theory of the resistivity of nanometric metallic structures arising from electron scattering by grain boundaries and by rough surfaces
Applied Physics Reviews **4**, 011102 (2017); 10.1063/1.4974032

100 years of the physics of diodes
Applied Physics Reviews **4**, 011304 (2017); 10.1063/1.4978231

Comparison of technologies for nano device prototyping with a special focus on ion beams: A review
Applied Physics Reviews **4**, 011302 (2017); 10.1063/1.4972262

Ion beam modification of two-dimensional materials: Characterization, properties, and applications
Applied Physics Reviews **4**, 011103 (2017); 10.1063/1.4977087

Effect of Joule heating and current crowding on electromigration in mobile technology
Applied Physics Reviews **4**, 011101 (2017); 10.1063/1.4974168

APPLIED PHYSICS REVIEWS

Adsorption-induced deformation of nanoporous materials—A review

Gennady Y. Gor,[1,a)] Patrick Huber,[2] and Noam Bernstein[3]

[1]*Otto H. York Department of Chemical, Biological, and Pharmaceutical Engineering,*
New Jersey Institute of Technology, University Heights, Newark, New Jersey 07102, USA
[2]*Institute of Materials Physics and Technology, Hamburg University of Technology (TUHH),*
Eißendorfer Str. 42, D-21073 Hamburg-Harburg, Germany
[3]*Center for Materials Physics and Technology, Naval Research Laboratory, Washington, DC 20375, USA*

When a solid surface accommodates guest molecules, they induce noticeable stresses to the surface and cause its strain. Nanoporous materials have high surface area and, therefore, are very sensitive to this effect called adsorption-induced deformation. In recent years, there has been significant progress in both experimental and theoretical studies of this phenomenon, driven by the development of new materials as well as advanced experimental and modeling techniques. Also, adsorption-induced deformation has been found to manifest in numerous natural and engineering processes, e.g., drying of concrete, water-actuated movement of non-living plant tissues, change of permeation of zeolite membranes, swelling of coal and shale, etc. In this review, we summarize the most recent experimental and theoretical findings on adsorption-induced deformation and present the state-of-the-art picture of thermodynamic and mechanical aspects of this phenomenon. We also reflect on the existing challenges related both to the fundamental understanding of this phenomenon and to selected applications, e.g., in sensing and actuation, and in natural gas recovery and geological CO_2 sequestration. © *2017 Author(s). All article content, except where otherwise noted, is licensed under a Creative Commons Attribution (CC BY) license (http://creativecommons.org/licenses/by/4.0/).* [http://dx.doi.org/10.1063/1.4975001]

TABLE OF CONTENTS

I. INTRODUCTION

By definition, adsorption is the enrichment of material or increase in the density of the fluid in the vicinity of an interface.[1] For any practical applications of adsorption, the high surface area is the key feature, which can be achieved when the adsorbent is porous. The discussion below concerns adsorption in *nanoporous* materials, which according to the IUPAC classification have pores with width below 100 nm.[2]

When studying adsorption, the discussion is usually focused on the influence of the solid component (adsorbent) on the adsorbed fluid (adsorbate). However, the converse action inevitably takes place—adsorbing fluid can exert colossal pressures (hundreds of atmospheres) on the solid, which leads to the deformation of the latter—adsorption-induced deformation. While experimental observations of adsorption-induced deformation of porous materials have

---

a)Author to whom correspondence should be addressed. Electronic mail: gor@njit.edu. URL: http://porousmaterials.net.

been known for centuries, the recent appearance of novel types of materials and new experimental techniques reignited the interest in this phenomenon. The main aims of the current review are the following:

1. Overview the seminal historical milestones in the studies of adsorption-induced deformation.
2. Summarize the most recent achievements in adsorption-induced deformation.
3. Review different experimental methods for measuring adsorption-induced strains.
4. Provide the up-to-date theoretical understanding of the physics of adsorption-induced deformation.
5. Specify the current and prospective application of this phenomenon.
6. Clarify key issues of future research studies.

Note, finally, that this review is devoted to adsorption-induced deformation of *nanoporous* materials. It does not cover the adsorption-induced stresses and strains in non-porous materials and discusses the phenomena at the plane surface only to introduce the concept of surface stress. There has been a vast literature on stresses at the plain surfaces induced by gas or electrolyte adsorption, many of which are summarized in a seminal review by Haiss.[3]

II. EXPERIMENTAL MEASUREMENTS OF ADSORPTION-INDUCED DEFORMATION

A. Macroscopic measurements

Experimental study of adsorption-induced deformation was initiated by the attempt of McBain and Ferguson in 1927 to understand the reason for swelling of various building materials with the increase of air humidity.[4] Using a gravimetric setup, they measured a series of water adsorption isotherms on sandstone, limestone, cement, etc. Although they did not perform strain measurements during the adsorption experiments, they concluded that the water adsorption is the cause of the materials' swelling.

In the same year, this study motivated Meehan[5] to carry out the first thorough measurement of adsorption-induced strains. Meehan studied another system: carbon dioxide adsorbing on charcoal. A precise measurement of charcoal expansion was a challenge, since the relative volumetric change is of the order of 0.1%. Meehan tried to perform volumetric measurements by displacement of mercury. However, this attempt failed, because mercury was entering the samples. Thus, Meehan switched to linear measurements. The charcoal samples were prepared in the form of 2-in. cubic blocks and placed in an optical lever-type extensometer. In such a system, the expanding sample rotates a small mirror, which translates to a large scale movement of a reflected light beam on a distant screen. In Meehan's installation, the screen was 8 feet from the mirror, so that a 10^{-3} in. strain of the sample corresponded to about 75 mm displacement of the beam. This allowed him to measure the deformations with very high precision. Meehan observed a monotonic expansion of the samples with the increase of gas pressure. These results are shown in Figure 1. Meehan also fitted the deformation curves obtained at different temperatures by simple analytical functions, but did not propose any theory.
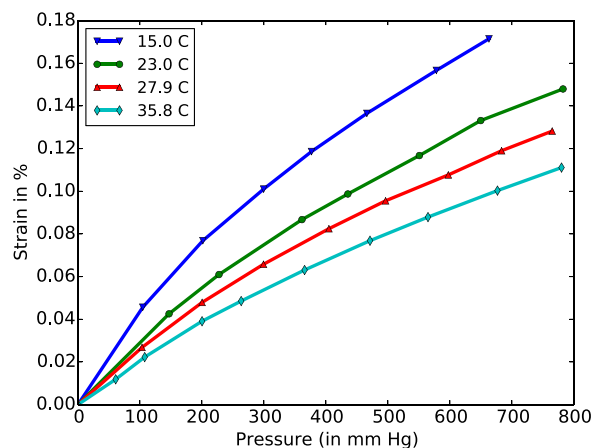

FIG. 1. Linear expansion of a charcoal sample induced by CO_2 adsorption as a function CO_2 pressure measured at different temperatures (top to bottom 15 °C, 23 °C, 27.9 °C, and 35.8 °C). Data from Ref. 5.

This challenge was immediately taken by Bangham and co-workers.[6] They carried out a substantial set of experiments on adsorption of various adsorbates (water, carbon dioxide, benzene, alcohols, etc.) on charcoal at different temperatures (see Ref. 7 and references therein) and observed a monotonic expansion of the sample with pressure growth. The explanation of the observations was the following: adsorption is a process which leads to surface energy reduction; therefore, the solid surface relaxes and tends to expand. So, the main conclusion made from these studies was that the expansion of an adsorbent is directly proportional to the reduction of free energy of a solid surface. This is what is now referred in the literature as *Bangham effect* or *Bagham's law*. A more detailed discussion of the Bangham effect is given in Section III A 1. Interestingly, roughly at the same time, following the pioneering experiments on charcoal, Briggs and Sinha performed dilatometric experiments during adsorption and desorption of methane and carbon dioxide on coal.[8] They also revealed monotonic expansion of samples upon adsorption with the maximal strain of the order of 10^{-3}. As was later understood, these effects have significant impact on methane extraction from the coal beds (see Section IV C).

In 1947, the experiments by Haines and McIntosh challenged Bangham's theory.[9] Dilatometric studies of the deformation of zinc chloride activated charcoal rods induced by adsorption of various organic vapors (butane, dimethyl ether, ethyl chloride) showed that Bangham's expansion takes place only above a certain gas pressure, corresponding to ~1/3 of the monolayer capacity. Below this pressure, in the initial region of the strain isotherm, a contraction of the samples compared to the evacuated state was observed. They also reported water adsorption and strain isotherms for one of the carbon samples. Both isotherms showed hysteresis (Figure 2), and the strain isotherm showed pronounced contraction on the desorption branch around 50%–70% humidity, which the authors interpreted as the formation of menisci in the capillaries during desorption.

The initial contraction of the samples at low gas pressures was further investigated by Lakhanpal and Flood in 1957.[10] They performed a study on various adsorbates
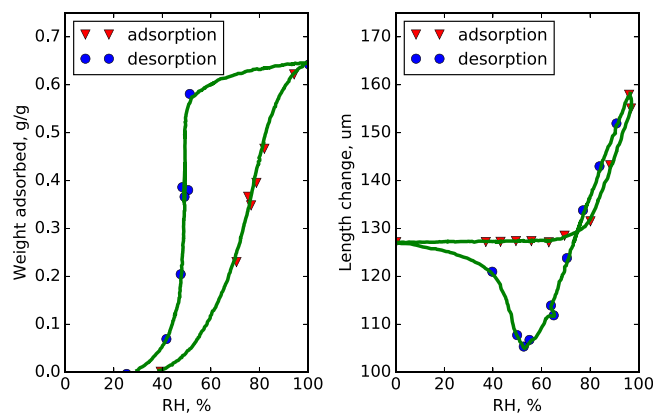
FIG. 2. Water adsorption on zinc chloride activated carbon at 20 °C. Left—adsorption isotherm, right—strain isotherm. Data from Ref. 10.

(ethane, n-propane, n-butane, 2,2-dimethylpropane, n-pentane, carbon tetrachloride, methanol) on activated carbon rods and observed the initial contraction for every single case. The initial parts of the isotherms from Ref. 10 are shown in Figure 3.

In the 1950s, the dilatometric studies on adsorption-induced deformation moved from carbons to porous glasses, commencing with a seminal work by Amberg and McIntosh.[11] They examined the deformation of Vycor glass induced by

adsorption of water vapor. The reported strain isotherm had two different regions of expansion separated by the region where contraction takes place (Figure 4). They gave a qualitative explanation for their experimental results based on both the Bangham effect and the Laplace pressure. However, it was hardly feasible to propose a quantitative model for their system. In order to do so, one would need to know the pores morphology, pore size distribution (PSD), etc.

Overall, within three to four decades after Meehan[5] had set the starting point of the adsorption/deformation studies and revealed difficulties in measuring the volumetric expansion, suggesting linear expansion, a significant amount of dilatometric measurements were accumulated for porous materials available at that time. A summary is given in Table I. Both for carbonaceous materials and glasses, the observed strains were of the order of 10^{-3}.

In the 1970s, dilatometric methods were also used for measuring the deformation of zeolite granules during adsorption of noble gases.[12,44,45] These measurements showed strain isotherms similar to carbonaceous microporous adsorbents: an initial moderate contraction at low gas pressure, followed by a noticeable expansion, see Figure 5. Reported strains were of the order of 10^{-4}.

The next important step in the development of experimental knowledge of macroscopic deformation induced by adsorption was related to the works of Reichenauer and Scherer.[17,18] They reported deformation of silica aerogels upon nitrogen adsorption. Although the strain isotherms were similar to that of other mesoporous materials, they were noticeably different in magnitude. Due to the high porosity of aerogels (ca. 90%–99%), they have extremely low elastic moduli, and therefore the observed deformation reached 30% strains.[18] Based on their measurements, Reichenauer and Scherer proposed a method for extracting the pore size distribution from the adsorption data on highly compliant materials.[19] Another interesting work on aerogels was reported by Herman et al.; they used liquid helium as an adsorbent, so that given the low surface tension ($\gamma_{He} = 10$ mN/m) the forces were much lower and the strain was moderate.[26]

Recently, significant progress has been achieved by a team from the Zentrum für Angewandte Energieforschung
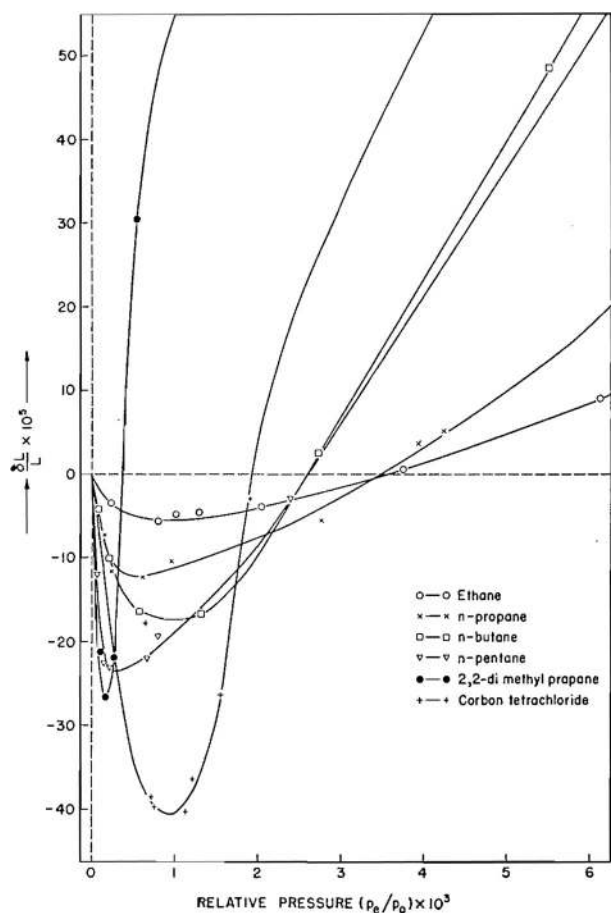

FIG. 3. Relative length change of an activated carbon rod at low pressure, showing initial contraction which takes place before Bangham's expansion. Reprinted with permission from Lakhanpal and Flood, Can. J. Chem. 35, 887 (1957). Copyright 1957 Canadian Science Publishing or its licensors.
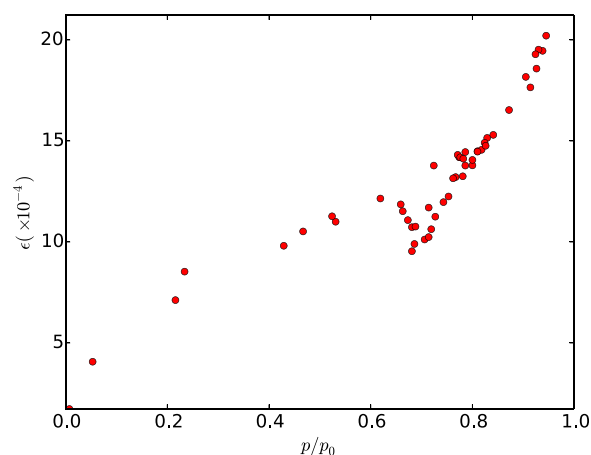

FIG. 4. Adsorption-induced strain of a Vycor glass sample due to water adsorption at 18.75 °C. Data from Ref. 11.

TABLE I. Key experimental studies on adsorption-induced deformation of nanoporous materials. The abbreviations "SAXS," "GISAXS," "WAXS," and "SANS" stand for small-angle x-ray scattering, grazing-incidence small-angle x-ray scattering, wide-angle x-ray scattering, and small-angle neutron scattering, respectively.

Year	Adsorbate	Adsorbent	Experimental technique	References
1927	CO_2	Charcoal	Optical lever extensometry	5
1928	H_2O, CO_2	Charcoal	Optical lever extensometry	6
1938	H_2O, CO_2, benzene, alcohols	Charcoal	Optical lever extensometry	7
1947	Butane, dimethyl ether, ethyl chloride,	Zinc chloride activated charcoal	Dilatometry	9
1952	H_2O	Mesoporous Vycor glass	Dilatometry	11
1957	Ethane, propane, butane, 2,2-dimethylpropane, pentane, carbon tetrachloride methanol	Activated charcoal	Dilatometry, optical microscopy	10
1977	Kr	Zeolite granules (CaNaX, LaNaX)	Dilatometry	12
1995	p-xylene	Zeolite (MFI)	WAXS	13
1996	Naphthalene	Zeolite (H-ZSM-5)	WAXS	14
	Pentane	Mesoporous silicon	WAXS	15
1997	p-nitroaniline	Zeolite (H-ZSM-5)	WAXS	16
2000	N_2	Silica aerogel	Dilatometry	17–19
	o-/m-xylene	Silicalite zeolites	WAXS	20
2002	H_2O	Natrolite, mesolite, scolecite zeolites	WAXS	21
	N_2	Mesoporous silica (MCM-41)	SAXS	22
	Toluene	Mesoporous silica	Ellipsometry	23
	H_2O	MOF (MIL-53)	WAXS	28
2005	H_2O	Mesoporous silica	Ellipsometry	25
2006	He, Ne	Aerogel	Dilatometry	26
2007	Perfluoro-pentane	Mesoporous silica (SBA-15)	SAXS	27
	CO_2	MOF (MIL-53)	WAXS	28
2008	H_2O	Thin mesoporous silica films	GISAXS	29
	Perfluoro-pentane	Mesoporous silica (MCM-41, SBA-15)	SAXS	30
	n-hexane, n-pentane, n-butane, n-propane, and SF6	Zeolites (NaA)	WAXS	31–34
2009	H_2O	Carbon nanotubes	Electron microscopy	35
2010	Electrolyte	Nanoporous gold	Dilatometry, WAXS	36
2011	N_2	Mesoporous carbon xerogels	Dilatometry	37
2014	H_2O	Thin mesoporous silica films	GISAXS	38
	Ar	Mesoporous Vycor glass	Dilatometry	39
2015	Hexane	Mesoporous silicon	Image analysis, optical interferometry	40
	H_2O	Mesoporous silicon	Dilatometry	41
	CO_2	Nanoporous carbon	SANS	42
	Pentane	Ordered hierarchical porous silica	Dilatometry, SAXS	43

Bayern;[37] unlike other groups which assemble *in situ* dilatometric setups from the scratch, Balzer *et al.* integrated a dilatometric setup into a commercial adsorption instrument. The setup is customized for rod-like samples with length in the centimeter range. The elongation is measured by a linear variable differential transformer sensor (LVDT) that provides a resolution of $\pm 0.2\,\mu$m, which for a 10 cm sample corresponds to the strain $\epsilon \sim 2 \times 10^{-6}$. It allowed them to utilize the quality of a well-established hardware and to achieve unprecedented resolution in gas pressure and ability to perform measurements for a variety of materials (e.g., Ref. 43).

Whereas in all previously discussed studies hosts with isotropic pore geometry were employed, recently two experiments on monolithic porous silicon with tubular pores parallel-aligned to the membrane surfaces were reported, see Fig. 6. This allows a simpler analysis and/or comparison with the theory as outlined in more detail in the theory section. Grosman *et al.*[40] employed image analysis and optical interferometry in order to measure the n-hexane adsorption-induced deformations of thin plates of porous silicon (with

55 μm thickness and lateral sizes of ca. 1 cm). They measured both the adsorption-induced strain along and transverse to the pore axis; this experiment is discussed in detail in Section II C. In the experiment by Gor *et al.*,[41] the macroscopic water-sorption induced deformation of porous silicon was measured by a linear motor stage, while a constant (small) axial tensile force was applied by a load cell during a continuous sweep of the humidity in the sample chamber.[41] Whereas qualitatively both experiments came to consistent results with regard to the deformation behavior and the hysteresis in the strain isotherm, they arrived at significant differences in the quantitative interpretation with regard to the elastic modulus of the silicon pore walls. Grosman *et al.* derived a Young modulus of the pore walls which is five times smaller than bulk silicon. By contrast, Gor *et al.* found a marginal reduction of the modulus by approx. 10%, only, a result which is consistent with inelastic neutron scattering experiments on the longitudinal acoustic phonons in mesoporous silicon.[46]

All of the above-mentioned methods required preparation of monolithic samples. However, some of the samples
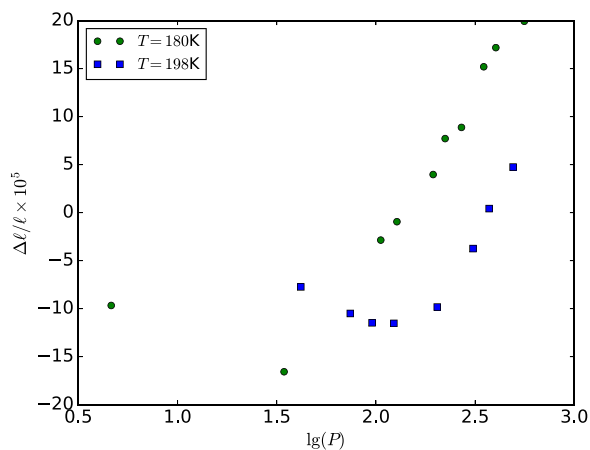
FIG. 5. Adsorption-induced strain isotherms (relative length change of a monolithic sample as a function of pressure) for krypton adsorption on CaA zeolites at 180 K and 198 K, digitized from the plots in Ref. 12.

cannot be prepared as monolithic material, such as thin low-dielectric-constant (low-k) films. A macroscopic approach for measuring adsorption-induced strains, alternative to dilatometry, was proposed by Mogilnikov and Balkanov[23] based on ellipsometric porosimetry (EP). Initially, EP was used as a method for measuring adsorption isotherms on thin low-k films, where the gravimetric and volumetric methods fail: the quantity of adsorbed fluid is calculated from a change of the refractive index during adsorption.[47,48] Additionally, this method gives the change in the thickness of the thin film during adsorption. Such measurements were proposed as a method for the determination of elastic properties of thin porous films; see Section III C for the detailed discussion. Clearly, EP is limited to measuring the strains in thin films and restricted to adsorbates with certain refractive indexes in combination with high vapor pressures; typically, toluene is used. The idea of using EP for measuring the elastic moduli of thin low-k films was further elaborated by Boissiere et al.[25] To interpret the experimental data, they used a generalized form of the Kelvin equation, taking into account Tolman's correction for the surface tension and the ellipsoidal shape of the pores. Figure 7 shows the film thickness of the
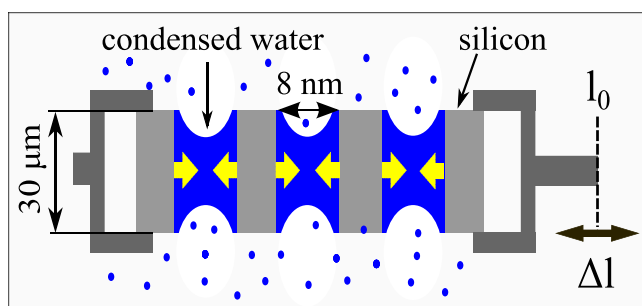

FIG. 6. Schematic of the experimental setup used for measuring the adsorption-induced deformation of porous silicon. The sample holder (dark grey, on the left) is connected to a load cell, and the sample holder on the right is connected to a linear motor stage to measure the length change δl. Lighter gray rectangles indicate solid pore walls, small blue dots indicate water vapor molecules, and regions bounded by curved blue menisci indicate condensed water. Yellow arrows indicate the force on the pore walls due to Laplace pressure. Reprinted with permission from Appl. Phys. Lett. **106**, 261901 (2015). Copyright 2015 AIP Publishing LLC.

porous silica film as a function of relative humidity for two subsequent adsorption-desorption cycles, changing as a result of adsorption-induced deformation.

The simplicity of macroscopic measurements of adsorption-induced strains and the sensitivity of these measurements to the pore sizes suggest that *in situ* dilatometry can be used as a tool for the characterization of porous materials.[37] Experimental strain isotherms can be treated similarly to an adsorption isotherm to derive the pore size distribution using a kernel of theoretical adsorption/strain isotherms.[49] Such a method could be especially efficient for the characterization of microporous samples, since the pressures and thus the strains are extremely sensitive to the pore sizes in this pore size range;[50] see the discussion in Section IV B. The limitation of *in situ* dilatometry is obvious and it is a consequence of its macroscopic nature: it does not work for powders, which is often a form of preparation of adsorbents or catalysts.

B. Strains on the microscopic scale

A new increase of interest in adsorption-induced deformation took place in the 1990s driven by the development of *in situ* X-ray and neutron scattering techniques. This new series of works started from a study by Dolino et al.,[15] where they reported the strains of crystalline porous silicon samples induced by adsorption of alkanes. X-ray diffraction (XRD) on crystals gives Bragg peaks which allow one to calculate the crystal lattice constants. Performing XRD on a porous sample *in situ* during an adsorption experiment revealed shifts of the Bragg peaks as a function of gas pressure, from which the strain isotherm for the crystal lattice was derived. Dolino et al. examined two different samples: a sample with 10 nm cylindrical pores and a sample with 3 nm spherical pores, according to their analysis. These samples resulted in two very different strain isotherms, shown in Figures 8 and 9. While the error bars on the second plot do not allow one to make quantitative conclusions from the data, the first plot
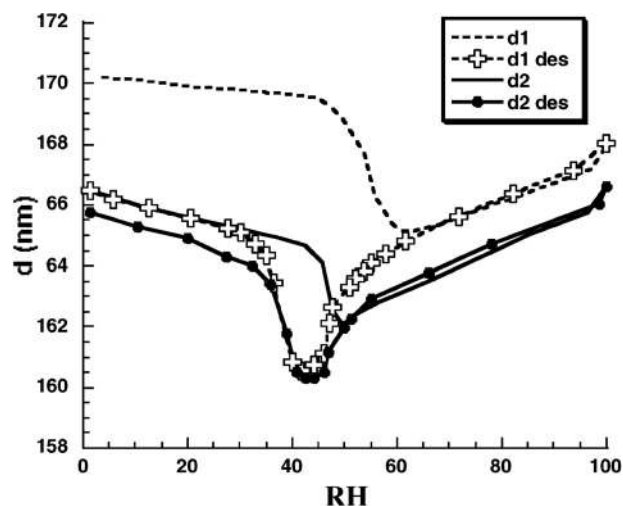

FIG. 7. Thickness of the porous silica film as a function of relative humidity of two sequential water adsorption-desorption cycles, changing as a result of adsorption-induced deformation. Reprinted with permission from Boissiere et al., Langmuir **21**, 12362 (2005). Copyright 2005 American Chemical Society.
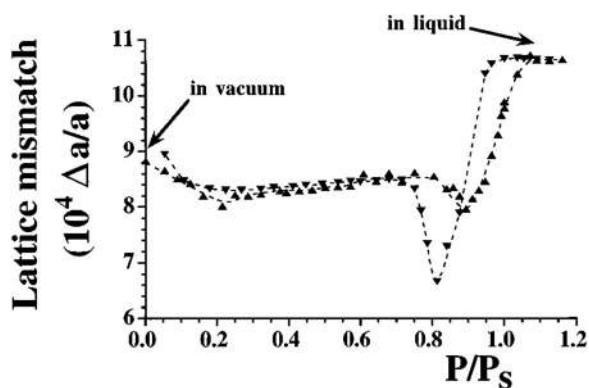
FIG. 8. Adsorption-induced strain measured as a relative change of the lattice constant in crystalline silicon with pores of ca. 10 nm diameter. This curve is similar to the one from macroscopic measurement on mesoporous glass, shown in Figure 4. Reprinted with permission from Dolino *et al.*, Phys. Rev. B **54**, 17919 (1996). Copyright 1996 American Physical Society.

is very similar to a typical strain isotherm measured by *in situ* dilatometry on a macroscopic sample, e.g., the data from Ref. 11 shown in Figure 4. Note that the strain isotherms for porous silicon measured by *in situ* dilatometry were reported almost two decades after the XRD data.[40,41] The only qualitative difference is the small contraction at low pressures. We will discuss this below in Section III E. Another porous crystalline system, investigated by *in situ* XRD was nanoporous gold, which will be discussed in Section II C.

Further progress in adsorption/deformation studies was governed by the revolution in materials synthesis related to the appearance of template-grown mesoporous silica: MCM-41[51,52] and SBA-15.[53,54] Although on the atomistic scale these materials are amorphous silica, they have an ordered structure on the mesoscale. Synthesis of these materials is based on using micellar aggregates as templates; therefore, the resulting materials can have a hexagonal (MCM-41, SBA-15) or cubic (SBA-16) lattice of pores, which is determined by the spatial arrangements and shape of the micelles. A lattice of pores gives Bragg peaks at positions typical of the structure factor of the pore lattice in small angle X-ray scattering experiments (SAXS)[52,54,55]—see Fig. 10.
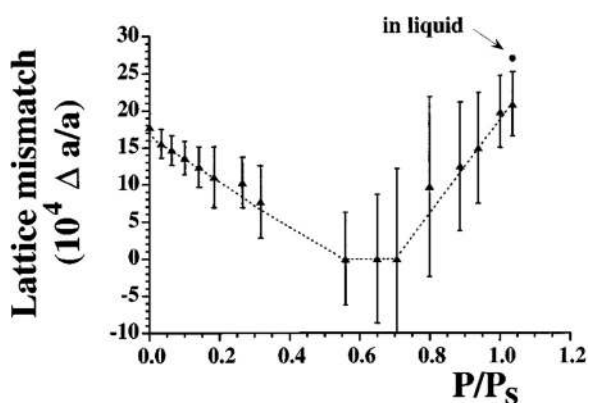

FIG. 9. Adsorption-induced strain measured as a relative change of the lattice constant in crystalline silicon with pores of ca. 3 nm diameter. Although large error bars complicate making quantitative conclusions, qualitatively, the shape of the curve resembles the one for zeolites (see Figure 5). Reprinted with permission from Dolino *et al.*, Phys. Rev. B **54**, 17919 (1996). Copyright 1996 American Physical Society.

Additionally, the form factor of the pores and thus the intensity of the Bragg peaks change in a distinct manner as a function of pore filling. Thus, ordered mesoporous materials are very suitable for studies of fluid adsorption. Template-grown silica and other self-ordered mesoporous substrates, such as ordered porous alumina, were intensively explored by *in situ* X-ray[22,56–60] and neutron scattering[61–63] studies during adsorption of various fluids.

The first to point out the adsorption-induced change of the pore lattice constant in ordered silica were Albouy and Ayral:[22] they noticed small shifts in the Bragg peaks during nitrogen adsorption in MCM-41. The thorough investigation of this effect using X-rays from synchrotron radiation was done later by Paris and co-workers[27,30,65] for MCM-41 and SBA-15 silica upon water, n-pentane, and perfluoropentane adsorption. From the Bragg peak shifts, they calculated the relative change of the pore lattice constant as a function of gas pressure, i.e., strain isotherms on the microscale; yet on a different scale than it was done by Dolino *et al.*,[15] since it corresponds to the *pore lattice* (~nm) and not the *crystal lattice* (~Å). It is worth noting that despite this difference, the
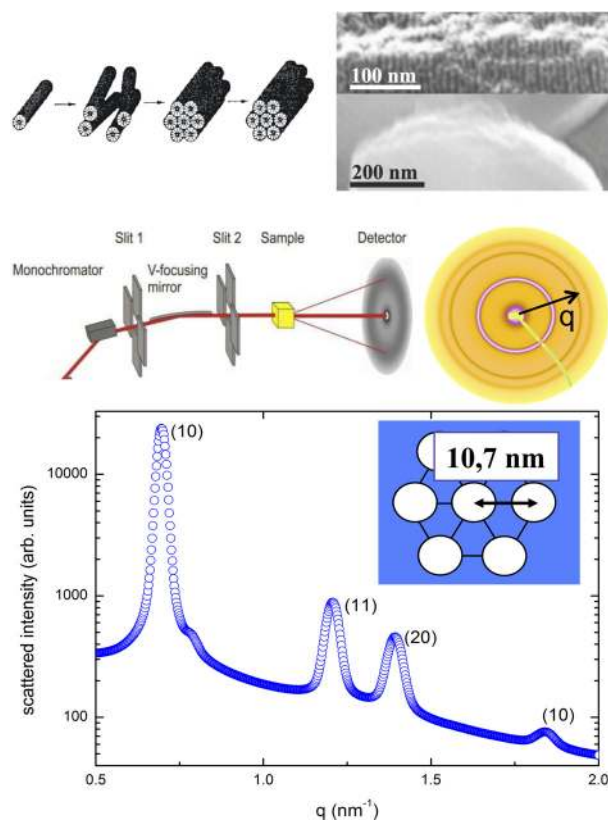
FIG. 10. SAXS experiment on a template-grown mesoporous SBA-15 matrix with a hexagonal arrangement of cylindrical pores: (a) Illustration of the templating process via hexagonal micelle arrangement. (b) Electron micrographs of a SBA-15 grain recorded with two magnifications as indicated in the figure.[64] (c) Schematics of the synchrotron-based SAXS experiment (left) and SAXS intensity rings typical of the powder diffraction pattern of SBA-15. (d) SAXS diffraction pattern characteristic of an empty SBA-15 powder. Plotted is the diffracted x-ray intensity versus the modulus of the wave vector transfer q. The Bragg peaks are indexed based on a 2D-hexagonal mesh with a 10.7 nm pore-pore distance as illustrated in the inset. The SAXS experiment was performed at PETRA III, beamline P03 of the Deutsche Elektronen-Synchrotron DESY, Hamburg, Germany. Courtesy of D. Rau, T. Hofmann, and P. Huber.

strain isotherms reported in Refs. 30 and 65 resemble those of Dolino *et al.* and the strain isotherms obtained using a macroscopic method, see Figure 11 and compare with Figures 4 and 8. However, there is a pitfall with regard to this experimental technique: besides the "real" lattice deformation due to the interaction of the solid pore walls with the fluid, an "apparent" lattice expansion was sometimes found experimentally in *in situ* adsorption SAXS experiments.[27] It results from a naive identification of all Bragg peak shifts with changes in the pore lattice constants, while ignoring alternative reasons for peak shifts upon fluid adsorption. In particular, the pore form factor changes during capillary condensation owing to the sequential filling of pores according to their diameter. Together with the structure factor from a lattice of finite size, this can lead to an effective shift of the Bragg peaks despite an unchanged pore lattice constant. This can be misinterpreted as an adsorption-induced deformation and thus as an "apparent" lattice strain.[66]

Another type of ordered porous materials is zeolites. Mechanical effects of adsorption on zeolites have also been investigated using XRD in 1990–2000. Mentzen and Gelin found that the lattice of MFI zeolite changes after p-xylene adsorption.[13] Van Koningsveld and Jansen reported the deformation of H-ZSM-5 zeolite upon adsorption of naphthalene[14] and p-nitroaniline.[16] Nair and Tsapatsis[20] also reported noticeable deformation of the silicalite lattice after adsorption of o-xylene and m-xylene. Expansion of zeolites of the natrolite family in the course of water adsorption was observed through *in situ* XRD experiments.[21] None of these studies, however, presented strain isotherms, but rather gave a comparison of XRD patterns before loading and after loading of the adsorbate. Later, Noble and Falconer investigated the change of the unit cell as a function of adsorption of various species[31–34] (these works are further discussed in Section IV C). They presented a strain isotherm for NaA zeolite membrane for a i-butane/methanol mixture (as a function of methanol activity) in Ref. 34. The reported trend, initial contraction followed by expansion, is the same as for the dilatometric measurements of zeolite granules.[12] To our

knowledge, there has been no strain isotherms for zeolites obtained with *in situ* XRD with a resolution comparable to the strain isotherms for silica.[30,65]

In the 2000s when a new type of porous materials, metal-organic frameworks (MOFs), gained its popularity, XRD studies on that material also revealed adsorption-induced deformation behavior. Moreover, some of the MOFs show extremely large strains—up to 30%, accompanied with a change of the crystalline structure. As such, Serre *et al.* synthesized MIL-53 MOF and by performing XRD on dry and hydrated samples found a huge change in the structure,[24] and further reported the changes in diffraction patterns with a change in the pressure of adsorbing CO_2.[28] Another example of significant adsorption-induced structure change of MOF DUT-49 was reported recently in Ref. 67. However, *in situ* XRD on some other MOF types shows strain isotherms during adsorption that are similar to conventional mesoporous materials.[68]

Unlike the *in situ* dilatometry, which does not work for measuring the adsorption-induced strains in thin films, *in situ* techniques using X-rays are capable of doing it. Dourdain *et al.* used *in situ* X-ray reflectivity to measure the strain isotherms for water adsorption on mesoporous silica films and suggested to use these measurements for deriving the elastic properties of thin films.[29]

To our knowledge, *in situ* X-ray scattering techniques applied to the adsorption/deformation behavior have not been performed on porous carbonaceous systems. Recently, however, *in situ* small angle neutron scattering was employed to measure the adsorption-induced deformation of microporous carbons.[42] This study showed that the adsorption of CO_2 on microporous carbons caused changes of the pore size up to 40% (from 5 Å to 7 Å). In addition to the unprecedentedly high strains, the shape of the strain isotherm was also qualitatively different from a typical shape for microporous materials. Finally, it is worth mentioning another measurement of adsorption-induced deformation on the microscale: Rossi *et al.* used environmental scanning electron microscopy and observed shrinkage of carbon nanotubes (CNTs) during capillary condensation of water vapor inside them.[35] Analysis of these measurements based on the generalized Young-Laplace equation allowed them to estimate the circumferential Young's modulus of the CNTs.

C. Beyond measuring one strain

All of the aforementioned experiments report measuring of linear strains in a certain direction, often chosen based on the sample dimensions. For disordered isotropic porous materials, like Vycor glass, such single measurement is sufficient to describe its elastic response to adsorption stresses.[69] However, for materials where the pores have a certain selected orientation, e.g., long parallel channels as in porous silicon, MCM-41 or SBA-15 silica, an isotropic behavior cannot be expected and therefore measurements beyond one strain are essential.

Sharifi *et al.*[38] investigated the deformation of thin (100 nm and 500 nm) mesoporous silica films during water vapor adsorption. These materials have cylindrical pores, oriented in the plane of the film. The authors used *in situ*
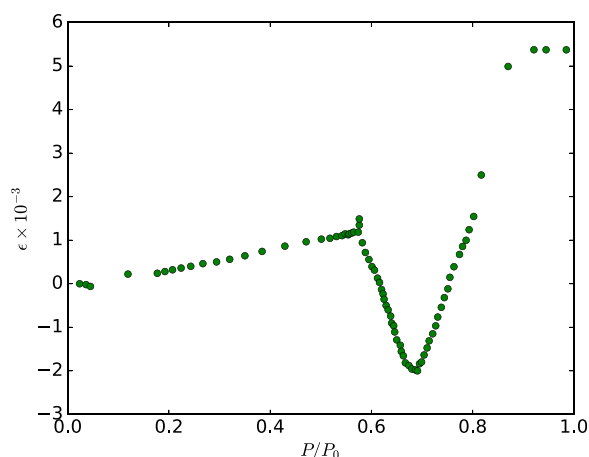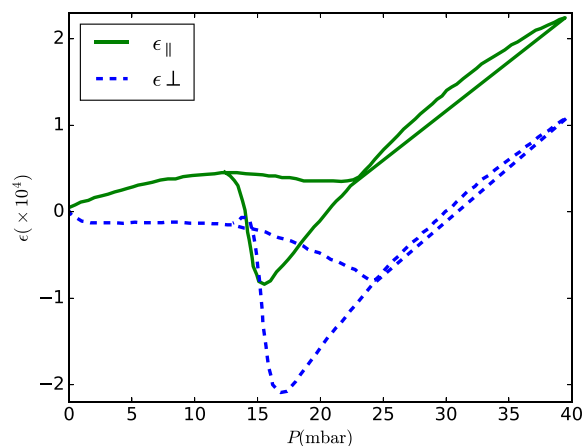

FIG. 11. Adsorption-induced strain measured from the shift of the Bragg peaks in *in situ* SAXS during water adsorption on SBA-15 silica at room temperature; data from Ref. 65.

FIG. 12. Strains in a mesoporous silicon wafer during n-heptane adsorption measured in two directions: $\epsilon_\parallel$—along the channel-like pores and $\epsilon_\perp$—normal to the pore walls. Data from Ref. 40.

grazing-incidence small-angle X-ray scattering to measure the change of in-plane and out-of-plane lattice parameters as a function of relative humidity.[38] The out of plane strain, similar to previous experiments,[30,65,70] showed a linear expansion in the beginning. The in plane strain is different, clearly showing linear contraction at higher pressures (then higher contraction near capillary condensation and finally expansion). Such a shape is similar to the measurements by Mogilnikov and Baklanov[23] and will be discussed below in Section III E.

As already mentioned in Section II A, Grosman et al.[40] used in situ dilatometry and reported strains parallel and perpendicular to the tubular pores in a mesoporous silicon film induced by heptane adsorption. The strain isotherms from this work are shown in Figure 12. The strain in the vertical direction resembles the strain isotherm on the mesoporous silicon sample measured using in situ XRD by Dolino et al.[15] (Figure 8), except that the initial contraction at low pressures is not observed. The lateral strain (normal to the pore axis) after capillary condensation is similar to the vertical strain; however, before capillary condensation, the behavior is qualitatively different: noticeable monotonic compression is observed. The possible reason for this behavior will be discussed in Section III E.

Sections II A and II B over-viewed two options for measuring adsorption-induced strains in porous materials:

materials which can be prepared as monolithic samples can be investigated by in situ dilatometry and materials which have ordered structure (be it atomistic or meso-scale order) are suitable for in situ XRD technique. Therefore, monolithic materials with ordered structure can be subjected to measurements of adsorption-induced strains on both scales. This was first implemented by Shao et al.[36] for electrosorption: a sample of nanoporous gold was immersed in aqueous electrolyte, and the response of the matrix as a function of electrode potential was measured using in situ dilatometry and wide angle X-ray diffraction. Thus, the system considered in that work was slightly different, yet very similar to the other systems discussed in the current review. The strain isotherms were obtained as a function of electrical potential and showed identical trends, but different magnitudes: microscopic strain $\epsilon \simeq 0.02\%$ and macroscopic strain $\epsilon \simeq 0.04\%$. The mismatch of these two values with application of a simple elastic model allowed the authors to conclude that the concept of fluid pressure is not sufficient to explain the deformation of porous solid, and the surface stress in the solid has to be taken into account. This issue will be further discussed in Section III E.

Recently, Balzer et al. performed macro- and microscale measurements of strains induced by adsorption of n-pentane in hierarchical silica monolith samples.[43] Unlike mesoporous silica of the MCM and SBA families, which is prepared in the form of powders, this material can be synthesized as a monolith (Figure 13). It is composed of a system of struts, each having a well-defined ordered structure on the mesoscale, similar to that of SBA-15 material. This unique structure provides an opportunity to measure both the macroscopic strains and the strains of the mesopore lattice from the shifts of the Bragg peaks by in situ SAXS. Figure 14 shows that both measurements give similar strain isotherms, which differ only in magnitude. This unique set of data allows one to understand how the strains on the pore scale are transformed to the macroscopic strains.

III. THEORY OF ADSORPTION-INDUCED DEFORMATION

A theory of adsorption-induced deformation should necessarily answer two main questions:
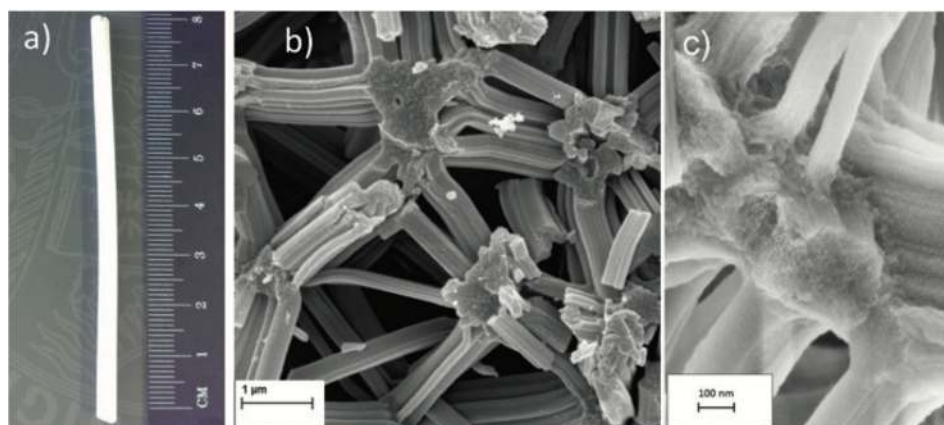

FIG. 13. Hierarchical silica monolith: (a) photograph of a sample, (b) and (c) SEM micrographs showing the structure of macropores between the struts and mesoporous structure of the struts. Scale bars on (b) and (c) are 1 μm and 100 nm respectively. Reprinted with permission from Balzer et al., Z. Phys. Chem. **229**, 1189–1209 (2015). Copyright 2015 Degruyter.
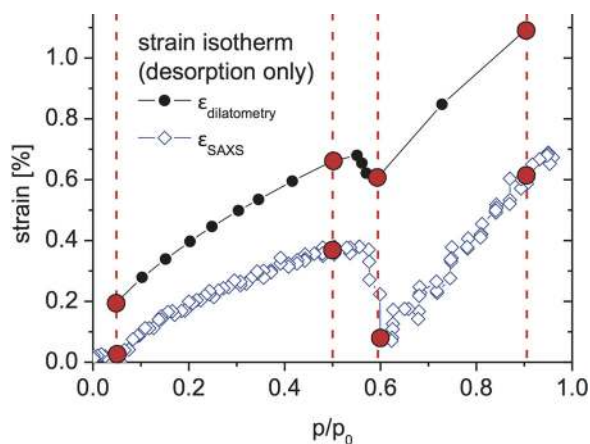
FIG. 14. Deformation of hierarchical silica monoliths upon pentane adsorption measured on two length scales: macroscopic (dilatometry) and microscopic (*in situ* SAXS). While the two measurements differ, they show very similar trends. Reprinted with permission from Balzer *et al.*, Z. Phys. Chem. **229**, 1189–1209 (2015). Copyright 2015 Degruyter.

1. How to predict the *stresses* in the pores induced by the fluid adsorption?
2. How do these stresses affect a porous material, so that the resulting *strains* are observed?

In a general case, these two questions cannot be addressed separately, since they are coupled: fluid adsorption and the stress that it causes depend on the strain of a surface. However, since for most materials the strains are very low, these questions can be decoupled and solved separately, which is discussed in Section III A and III B. After that, various approaches taking into account the coupling effects are discussed.

A. Qualitative theories

1. Monotonic expansion: Bangham's law

The first theoretical explanation of adsorption-induced deformation was given by Bangham. Based on a series of experiments,[71–74] which all showed monotonic expansion of charcoal samples with increased adsorbate pressure, Bangham concluded that the measured linear strain ϵ is proportional to the decrease in the surface energy γ of a solid, caused by adsorption

$$\epsilon \propto \Delta\gamma. \qquad (1)$$

According to the Gibbs adsorption equation, the surface energy of a solid surface γ decreases upon adsorption as[75]

$$d\gamma = -\Gamma d\mu, \qquad (2)$$

where Γ is the surface excess of the fluid component and μ is the fluid chemical potential. Using the ideal gas law and integrating Eq. (2), we get[76]

$$\Delta\gamma = \gamma - \gamma(0) = R_g T \int_0^p \Gamma d\log p, \qquad (3)$$

where R_g is the gas constant, T is the absolute temperature, and p is the vapor pressure. The difference $\Delta\gamma$ is often

referred to as the spreading pressure, and according to Eq. (2) or Eq. (3), it is obviously always negative. The negative $\Delta\gamma$ corresponds to the positive ϵ—monotonic expansion.

2. Contraction at low pressures

All experimental strain isotherms reported in 1920s–1930s showed only monotonic expansion of the samples with the increase in gas pressure (see Figure 1), and therefore, Bangham's effect was fully describing the observed phenomena. The appearance of more precise measurements from Haines and McIntosh[9] showed that the strain isotherms for microporous materials have a small region where the samples contract, which could not be explained by Bangham's equation (3). The contraction in the beginning of the strain isotherm was further confirmed in several other experimental works[10,77,78] and the following explanation was given by Lakhanpal and Flood.[10] Bangham's theory considers adsorption *on a surface* and *not in a pore*; in a micropore, the presence of an opposite wall changes the picture qualitatively. At low pressures in micropores, the adsorbate molecules may form a bridge between the opposite pore walls. The formation of such bridges causes the contraction. At higher pressures, when more molecules are introduced in the pore space, the interactions between the fluid molecules cause the disappearance of the bridges, and then the expansion of a sample is observed, governed by Bangham's law. Figure 15 presents a schematic of the bridging effect from Ref. 10. The physical bridging between the opposite walls is likely to take place if the walls have certain non-idealities, such as stronger adsorption sites, corrugated, or non-planar surfaces.

However, the physical bridging is not necessary to explain the initial contraction of micropores. Ash *et al.*[79] considered a model system of two parallel adsorbing plates and derived an expression for forces acting between them. According to them, the change of potential energy u of interaction between unit areas of plates, relative to zero at infinite distance between the plates, is given by

$$\Delta u = u - u_0 = -2R_g T \int_\infty^H \int_0^p \left(\frac{\partial\Gamma}{\partial H}\right)_{T,p} d\ln\left(\frac{p}{p_0}\right) dH. \qquad (4)$$

Here, u_0 is the potential energy of interaction between the dry plates, H is the separation between the plates (pore width), and p_0 is the pressure of the saturated vapor. The key question is the dependence of the adsorption isotherm $\Gamma(p, H)$ on the separation between the plates H. If we decrease H, there will be two competing effects: on the one hand, it will cause an increase of the overlap of the attractive potentials of the plates, increasing the total adsorption; on the other hand, when the volume between the plates is decreased, it tends to "squeeze the molecules out," reducing the adsorption. Depending on the relative contributions of these two factors, $\left(\frac{\partial\Gamma}{\partial H}\right)_{T,p}$ can be positive, causing the repulsion between the plates (expansion of the pore), or negative, causing the attraction between the plates (contraction of the pore).
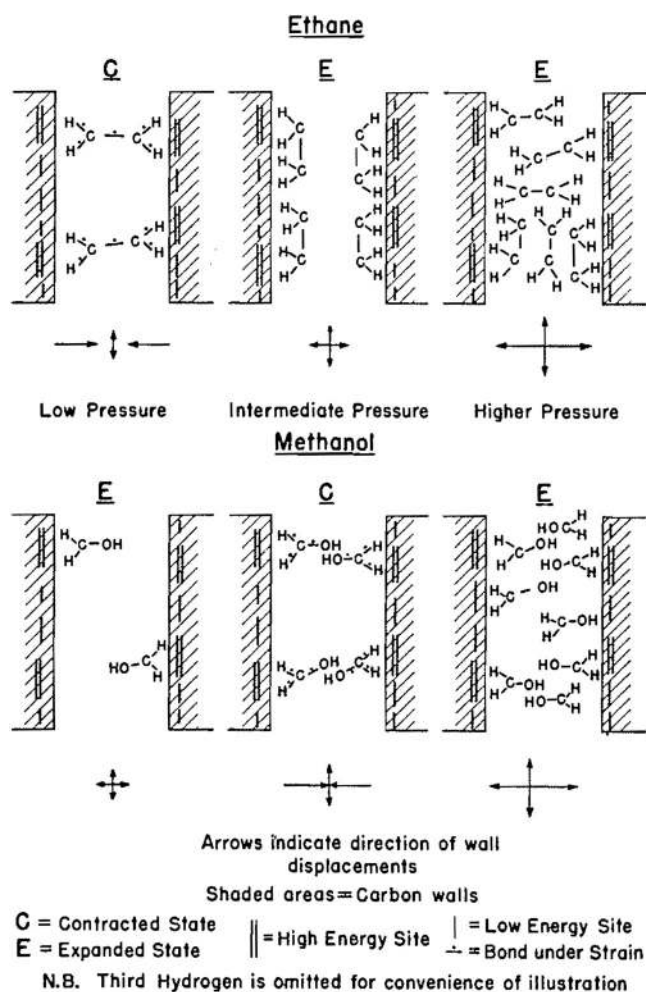
Ethane

FIG. 15. A sketch illustrating the idea of molecular bridging, which causes the contraction of micropores at low gas pressures. Reprinted with permission from Lakhanpal and Flood, Can. J. Chem. **35**, 887 (1957). Copyright 1957 Canadian Science Publishing or its licensors.

3. Mesoporous materials

Note that the aforementioned effects, monotonic expansion and contraction-expansion behavior, are related to microporous materials. Typical strain isotherms for mesoporous materials have more complicated shapes (see Figures 4 and 14). A qualitative and to some extent even quantitative theory of adsorption/deformation of mesoporous materials was given by Amberg and McIntosh along with the experimental measurements for Vycor glass (average pore size ca. 6 nm).[11] They explained the two different regions of the strain isotherms as the deformation due to "spreading pressure" (Bangham effect) before capillary condensation, and due to Laplace forces at the concave menisci in the pores after the capillary condensation. In the transition region in between those two, it is assumed that the two different mechanisms compensate each other and no changes in strains are observed. This mechanism was further confirmed by a quantitative theory,[80] and will be discussed in detail in Section III B 2.

B. Quantitative thermodynamic theories

Substantial progress in experimental measurements of adsorption-induced deformation along with the progress in molecular modeling techniques has driven the development of theoretical models of adsorption-induced deformation in the 2000s. A number of papers employed molecular modeling techniques for predictions of adsorption-induced strains in various nanoporous materials: Monte Carlo simulations[40,81–92] or classical density functional theory (DFT).[93–96] At the same time, several purely analytical theories were also proposed.[80,97–101] Most of these papers, however, were still limited to qualitative comparisons with experimental data. Some successful examples of theories of adsorption-induced deformation, which provide quantitative agreement with experiment, are described below.

1. Microporous materials

Jakubov and Mainwaring[97] and later Ravikovitch and Neimark[94] proposed theories capable of calculating the adsorption stress for zeolites in good agreement with experimental data from Refs. 12, 44, and 45. The theory of Jakubov and Mainwaring is based on the vacancy solution theory[102] for calculation of adsorption stress and the use of Hooke's law to calculate strain from it.[103] The work of Ravikovitch and Neimark is based on DFT methods widely used in adsorption studies, and it was further extended for calculation of adsorption strains for various micro- and mesoporous materials; therefore, we present it here in more detail.

Their theory is based on the following assumptions:

1. The deformation of a porous sample (zeolite) is isotropic and described in terms of the engineering volumetric strain ϵ_V. Moreover, the density of the solid framework is unchanged and the volumetric strain is related solely to the change of the pore volume V, thus $\epsilon_V = \Delta V / V_0$, where V_0 is the volume of the dry pore. The pores are assumed to have spherical geometry with uniformly distributed adsorption sites, and all the pores have the same radius.

2. The stress-strain relation is given by Hooke's law for the volumetric strain

$$\sigma = M_V \epsilon_V, \tag{5}$$

where M_V is a certain volumetric elastic modulus. It is assumed that $M_V = K_p$, the bulk modulus of the porous material, i.e., the load is assumed to be similar to hydrostatic compression/expansion. A detailed discussion of the elastic constants relevant to adsorption-induced deformation is given in Section III C.

3. The free energy of the adsorbed phase in deformed pores is unaffected by the elastic free energy, and is calculated based on molecular theories of adsorption in a nondeformable pore.

4. The deformation is fully determined by "adsorption stress," the component of the pressure tensor normal to the pore walls, which is calculated as

$$\sigma_s = -\left(\frac{\partial \Omega}{\partial V}\right)_{\mu,T}, \tag{6}$$

where Ω is the grand thermodynamic potential of a *rigid* pore of volume V with adsorbed fluid in it. Therefore, the grand potential Ω can be calculated using some

well-established methods for modeling the adsorption. Ravikovitch and Neimark used the Non-local DFT (NLDFT) method for spherical pores,[104] and calculated the derivative in Eq. (6) as a finite difference. Note that consideration of only the normal component is an approximation. Many works report predictions for other components of the pressure tensor in confined fluids, and show that these values are noticeable, but the corresponding deformation is not considered.[105–107]

To be more precise, the driving force for the deformation in Eq. (5) was calculated as "solvation pressure" f_s, the difference between the pressure inside the pore σ_s and outside p. Note, however, that $p \ll \sigma_s$. The results of their calculations for the adsorption isotherm of Xe on CaNaX zeolite and the corresponding adsorption strain are given in Figure 16.[94] Theoretical predictions are consistent with the qualitative discussion in Section III A 2; moreover, they provide quantitative agreement with the experimental measurements, while using only one fitting parameter, the bulk modulus K_p in Eq. (5).

Despite the number of strong assumptions, this "thermodynamic approach" made it possible to calculate strain isotherms for various other microporous systems, e.g., activated carbons,[108] synthetic carbon monoliths,[50] coal,[95,109] and even breathing MOFs.[101] The key part is that

FIG. 16. Adsorption isotherms (top), solvation pressures and strains (bottom) for Xe adsorption on CaNaX zeolite. Experimental data, shown with diamonds, are from Ref. 44, theoretical predictions are from Ref. 94. Reprinted with permission from Ravikovitch and Neimark, Langmuir **22**, 10864 (2006). Copyright 2006 American Chemical Society.

the grand potential of the system (and therefore its derivative) is calculated based on a theory of adsorption in a *rigid* pore. The use of DFT is not necessary and various other approaches can be employed. For example, the strains in Ref. 108 are calculated based on grand canonical Monte Carlo (GCMC), and the strains in Ref. 101 are derived analytically based on the Langmuir theory of adsorption.

2. Mesoporous materials

Unlike in microporous materials, where the filling of pores during adsorption is a continuous process, adsorption in mesoporous materials takes place in two distinct steps.[1] During adsorption at low pressure, the fluid becomes adsorbed on the pore walls so that a multilayered liquid-like film grows. The thermodynamic properties of such a film are determined by the attractive interactions with the pore walls and surface tension γ_{vl} at the vapor-liquid interface. At a certain thickness h_c, the surface tension makes the film thermodynamically unstable and capillary condensation takes place so that the pore is filled with a liquid-like adsorbate. This corresponds to a certain pressure p_c, which strongly depends on the pore size. In the reverse process, when desorption takes place from a liquid-filled pore, the system passes the p_c point and equilibrium capillary evaporation occurs at the pressure p_e, at which the grand potential of a filled pore equals the grand potential of the pore with a liquid film of a certain thickness. The difference between p_e and p_c is the most common origin of hysteresis observed in adsorption isotherms in mesoporous materials. For detailed discussion on adsorption hysteresis, refer to the following review papers.[49,110–112] The first theory of adsorption in mesoporous materials capturing this physics was derived by Derjaguin,[113] and later proposed as a method for calculation of pore size distributions of porous materials by Broekhoff and de Boer.[114] In the 2000s when mesoporous molecular sieves appeared, the Derjaguin–Broekhoff–de Boer (DBdB) theory was confirmed quantitatively by experimental adsorption data on MCM-41 and SBA-15; it was also shown to be consistent with the predictions of adsorption based on density functional theory.[110] Figure 17, reproduced from Ref. 96 (top), shows the experimental adsorption isotherm for N_2 on SBA-15 silica and theoretical isotherms calculated for a 8.2 nm cylindrical silica pore using the DBdB theory and using the Quenched Solid DFT (QSDFT) method.[115]

Gor and Neimark employed the thermodynamic approach described in Section III B 1 together with the DBdB theory of capillary condensation to predict the adsorption-induced deformation of *mesoporous* materials.[80] Before presenting that result, it is necessary to introduce the basic idea of the DBdB theory. The key idea of Derjaguin's original approach is that a thin liquid film adsorbed on a solid surface has the density of the bulk liquid, but its chemical potential differs from that of a bulk liquid.[117] This difference is related to the so-called disjoining pressure Π, which is a function of the film thickness h. When the surface is curved (e.g., the fluid is adsorbed on the walls of a cylindrical pore with radius R), an additional term, corresponding to the Laplace pressure at the liquid-vapor interface, is included
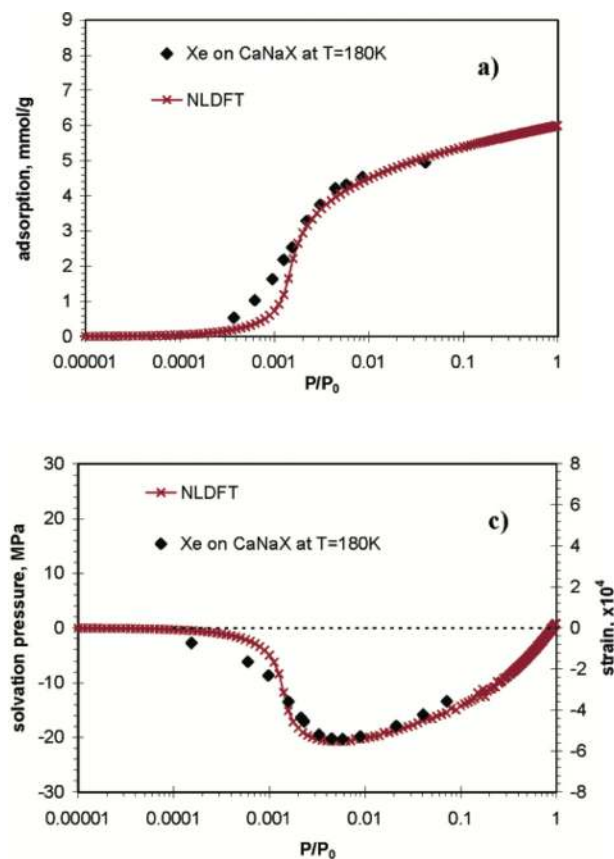
in the chemical potential. The total chemical potential is determined by the sum of those two contributions,

$$\mu = -v_l \left[\Pi(h) + \frac{\gamma_{vl}}{R - h} \right], \quad (7)$$

where v_l is the molar volume of the fluid (assumed to be the same as for the bulk liquid at a given temperature), $\Pi(h)$ is Derjaguin's disjoining pressure. Note that Eq. (7) does not include any terms related to the solid-liquid interface.

Based on Eq. (7), the expression for the grand potential Ω of the pore with the adsorbed fluid prior to the capillary condensation can be derived. One needs to differentiate the resulting expression for Ω to get the adsorption stress from Eq. (6). The corresponding derivation can be found in Ref. 80 and gives

$$\sigma_s(p) = -\frac{\gamma_s}{R} + \frac{\gamma_{vl}}{R} - \frac{\gamma_{vl}}{(R - h)} - \frac{h}{R} \Pi(h) + \frac{1}{R} \int_0^h \Pi(h')dh', \quad (8)$$

where γ_s is the surface energy of the dry solid. After capillary condensation, when the pore is filled with liquid-like fluid, and has a meniscus at the entrance, the adsorption stress is given by a simple expression,

$$\sigma_s(p) = -\frac{\gamma_{sl}}{R} + \frac{R_g T}{v_l} \ln\left(\frac{p}{p_0}\right). \quad (9)$$

The second term in Eq. (9) is the Laplace pressure at the vapor-liquid interface expressed using the Kelvin-Laplace equation. The first term is related to the interface energy at the solid-liquid interface γ_{sl}, which is different from γ_s. Although this term is a constant, it has an important contribution to the observed deformation: the final stress at saturation $p = p_0$, when the pores are completely filled, is different from the initial stress.

Eq. (8) is derived from the change in the grand potential of a dry pore when the adsorbed fluid forms a thin film on the pore walls. Eq. (9) is derived based on the change in the grand potential of a pore which is fully filled with fluid. While the former is written in terms of the surface energy of solid surface γ_s, the latter is expressed using the surface energy of the solid-liquid interface γ_{sl}. To relate these two quantities in Ref. 80, the Frumkin-Derjaguin equation[113,117,118] was used

$$\gamma_s - \gamma_{vl} - \gamma_{sl} = \int_0^\infty \Pi(h')dh'. \quad (10)$$

Eqs. (8)–(10) allow one to predict the solvation pressure as a function of p/p_0 in the whole range from $0 \le p/p_0 \le 1$. The result from Ref. 96 is shown in Figure 17 (bottom) for the case of N_2 adsorption on silica. The DBdB theory provides perfect agreement with the calculations based on QSDFT. The experimental strain isotherms for this system were not available; however, comparison of the theoretical predictions with experiments was done for a different system—strains
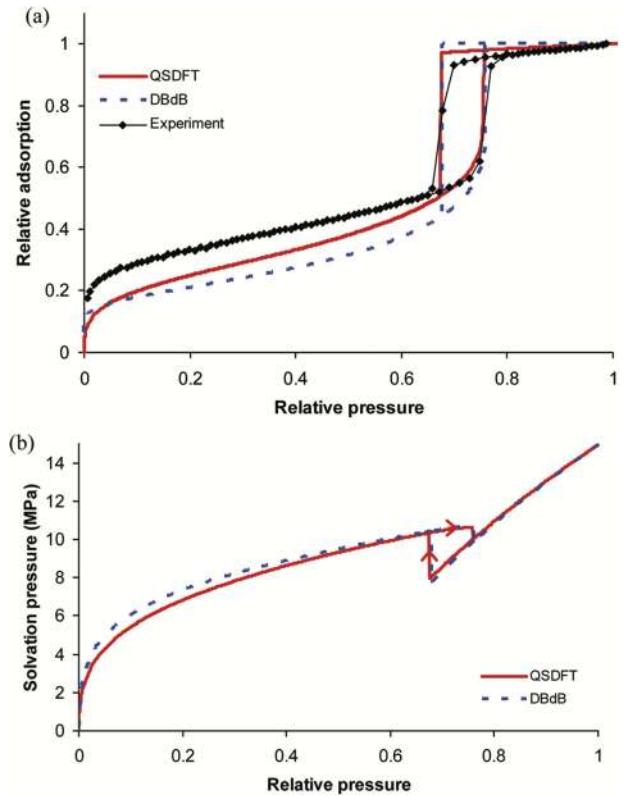

FIG. 17. Adsorption of nitrogen on mesoporous silica at 77 K from Ref. 96. Top: adsorption isotherms, experimental isotherm for SBA-15 silica with 8.2 nm pore size from Ref. 116 and calculated isotherms based on QSDFT and DBdB theories. Bottom: solvation pressure isotherms predicted for this system based on a thermodynamic approach. Reprinted with permission from Gor and Neimark, Langmuir **27**, 6926 (2011). Copyright 2011 American Chemical Society.

induced by n-pentane adsorption on MCM-41 silica. To calculate the strain from the solvation pressure, a single elastic constant was used (Eq. (5)), which was a fitting parameter based on the experimental data after capillary condensation, where it has a simple logarithmic form. The resulting comparison is shown in Figure 18.
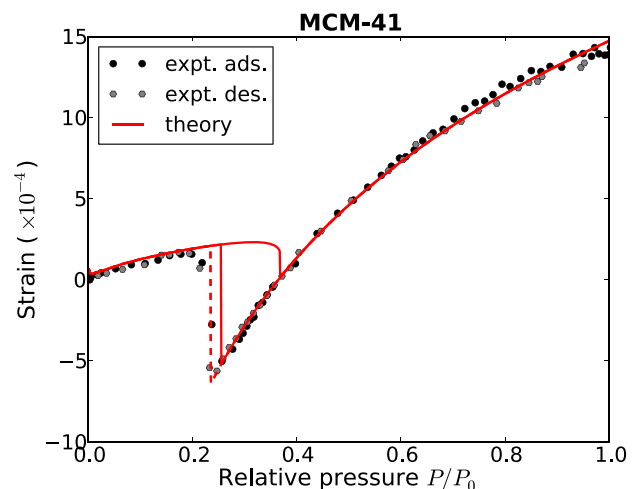

FIG. 18. Adsorption-induced strain isotherm for n-pentane adsorption on MCM-41 silica. Circles represent the experimentally measured strain from *in situ* SAXS and lines represent theoretical calculations based on Eqs. (8) and (9). Reprinted with permission from Gor *et al.*, Langmuir **29**, 8601 (2013). Copyright 2013 American Chemical Society.

C. Elasticity of adsorption-induced deformation

While the thermodynamic approach overviewed above gives a recipe for calculating the pressure in the pore (or adsorption stress), it leaves the elastic modulus M in Eq. (5) as a fitting parameter. However, in order to give the theory a full predictive capability, it is necessary to have an expression for this so-called pore load modulus[65] as a function of the underlying physical parameters, in particular, the elastic properties of the solid matrix and the pore structure (volume fraction, size, and shape of the pores). This is of utmost importance when the adsorption strain data is used specifically for an estimation of elastic properties of a material,[23,25,29] as discussed further in Section IV B.

The first attempt to get the relation between the pore load modulus M measured from the adsorption strain isotherms and conventional elastic constants of the materials was made by Bangham and Maggs.[119] They considered adsorption-induced deformation as an elongation of a thin rod, which has a surface area per unit mass equal to that of the porous solid, by the tangential stress from the Bagham effect, and thus related M to the bulk solid's Young's modulus. Yates proposed to relate the expansion constant to the bulk modulus, assuming that the porous material behaves like an aggregate of sintered spheres.[120] Scherer derived the equation for the pore load modulus for a porous glass, taking into account its microstructure, assumed to be a system of cylindrical rods.[121] The dependence of the pore load modulus on the microstructure is crucial, and therefore the application of Scherer's equation, derived for Vycor glass, to porous materials having different microstructure may give unsatisfactory results.[15] Many materials (porous silicon, porous alumina, mesoporous silica of various types) have a microstructure of a bundle of parallel cylindrical channels in the mesopore size range. An example of such a microstructure in mesoporous silicon is shown in the SEM image in Figure 19. Because this geometry is so common, we now review the calculation of the pore load modulus for this microstructure in more detail.

Recently, Prass *et al.* reported experimental measurements of adsorption-induced strains by *in situ* XRD on several different MCM-41 silica samples.[65] They also simulated the deformation of a hexagonally ordered porous structure (representing the structure of MCM-41) by the finite element method (FEM) for continuum elasticity. Finally, they proposed that the strain, derived from the change of the lattice parameter of the hexagonal lattice of pores, behaves similarly to the hoop stress in a single thin-walled cylinder, and gave an analytical expression for the pore load modulus. Although that model provided good agreement with their experimental data, it was not consistent with their FEM calculations.

An improved model for the pore load modulus was presented recently.[41] This model does not employ the thin-wall assumption, and is fully consistent with FEM calculations. The idea of this model is that the adsorption-induced normal strains in the materials composed of parallel, channel-like pores can be calculated based on the displacement of the external surface of a single *thick-wall cylinder*. The left panel in Figure 19 shows the structure of porous silicon, and the central and right panels show the model structure from Ref. 41. Note that the idea of representing a porous material as a thick-walled cylinder was proposed earlier by Rusanov and Kuni,[99,100] but neither verified by FEM calculations nor compared to experimental data, as was done in Ref. 41. This simplification makes it possible to write the pore load modulus M as a function of Young's modulus E and Poisson's ratio ν of the *non-porous* solid matrix, and the porosity ϕ (defined as the ratio of the volume of the pores to the overall volume of the porous solid)

$$M = \frac{E}{2(1-\nu^2)}\left(\phi^{-1} - 1\right). \tag{11}$$

Note that for mesoporous materials the estimation of pore load modulus is especially straightforward in the region after the capillary condensation, when the change of the adsorption stress is governed by the Laplace pressure and the strain has a simple logarithmic dependence on gas pressure p/p_0 (Eq. (9)). In Ref. 41, the model of Eq. (11) was compared to experimental data for adsorption-induced deformation of porous silicon and showed reasonable agreement. Here, we compare this model to the experimental data for MCM-41 silica,[65] which has an ordered hexagonal lattice of
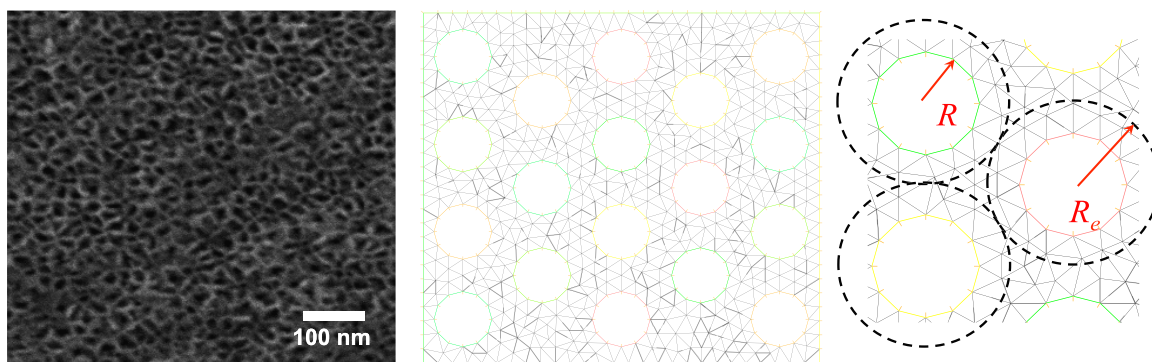
FIG. 19. Structure of porous silicon seen in SEM image (left) and its finite element representation (center) used in model from Ref. 41. This model considers a two-dimensional structure with the circular pores distributed on a hexagonal lattice. The FEM analysis suggests that the elastic response of such structure to the load in the pore is close to the response of the cylindrical domains (zoomed-in view in right panel) in the R_e vicinity of each pore; the latter problem can be solved analytically. Reprinted with permission from Appl. Phys. Lett. **106**, 261901 (2015). Copyright 2015 AIP Publishing LLC.

mesopores. The pore load modulus calculated using Eq. (11), calculated by FEM simulations of a hexagonal lattice of pores (similar to the ones in Ref. 41), and derived from experimental data for MCM-41 silica of Ref. 65 are shown in Figure 20. Poisson's ratio $\nu = 0.17$, typical of amorphous silica, was used in the calculations, and Young's modulus of the pore walls E was left as a fitting parameter. Clearly, as shown in Figure 20, there is an excellent agreement between the experimental data and the model, which proves that Eq. (11) captures the porosity dependence of the pore load modulus very well. Note, however, that the best agreement was achieved using $E = 44$ GPa in the calculations, which is significantly lower than the value of 73 GPa of bulk amorphous silica. This observation suggests that Young's modulus of the pore walls of MCM-41 silica may be noticeably lower than the bulk.

The pore load modulus is different from the bulk modulus of a porous structure: the former describes adsorption-induced deformation of the material due to a pressure applied on the pore walls, while the latter describes the deformation of the material due to a hydrostatic pressure acting on the external surfaces. Moreover, the dependence of the pore load modulus on porosity (Eq. (11)) qualitatively differs from the dependence of the bulk modulus K_p or Young's modulus E_p of the porous structure. The dependence of the latter is often well described by the Gibson-Ashby relation[122,123]

$$E_p = \tilde{E}(1 - \phi)^2, \tag{12}$$

where $\tilde{E}$ is a certain constant, not necessarily equal to E. Therefore, the model for derivation of Young's modulus of a porous film from the adsorption strain[23] has to be revised to take into account the difference between the pore load modulus and Young's modulus. The same applies to the recent work by Grosman et al.;[40] the authors derived Young's modulus of the pore walls of mesoporous silicon based on the pore load modulus calculated from the heptane adsorption data. However, the incorrect assumption of the dependence of the pore load modulus on the porosity led them to an

apparent Young's modulus for the silicon matrix which was several times lower than the bulk value. This is in contrast to most recent inelastic neutron scattering experiments on the longitudinal acoustic phonons in the silicon matrix, which indicate only a slight reduction of Young's modulus of the Si walls compared to bulk Si.[46]

The two-dimensional model for the pore load modulus[41] presented above has recently been generalized to take into account additional surface elastic constants.[124] Such additional constants could be introduced for nanoscale solids, where elastic properties can deviate from their bulk values. However, for mesoporous materials, where the characteristic pore size and pore wall thickness are of the order of several nanometers, these deviations are likely to be negligible. This is in line with the result of Ref. 124, which differs from the pore load modulus from Ref. 41 insignificantly. Additionally, Liu et al. proposed a pore load modulus model for composite materials with pores coated with a surface layer with different mechanical properties.[125]

D. Coupling between thermodynamic and elastic aspects of adsorption-induced deformation

Strictly speaking, strain affects the adsorption properties of the material; however in most cases, the strains induced by adsorption are small and therefore the calculation of the pressure in the fluid (which depends on adsorption) and the resulting strain can be uncoupled. Nevertheless, a number of theoretical studies have been performed to consider these usually neglected effects. A qualitative model by Ash et al.[79] included this coupling through the derivative of the amount adsorbed Γ by the width of a slit pore H, $(\frac{\partial \Gamma}{\partial H})_{T,p}$. Shen and Monson performed a Monte Carlo simulation study of gas adsorption in a semiflexible porous network with a high porosity (over 95%) to represent this process in silica aerogels.[81] In addition to qualitatively reproducing the observed adsorption-induced deformation, they showed that network flexibility significantly alters the adsorption and desorption isotherms as compared to a rigid network. Schoen and co-workers[83,84] performed a Monte Carlo simulation study for a model system, Lennard-Jones (LJ) fluid adsorption in a slit pore, where the solid atoms were allowed to elastically depart from their equilibrium sites, by a harmonic potential. Such a system is able to be strained normal to the pore walls, changing the width of the slit pore. They also reported the change of thermodynamic properties of the fluid compared to the same fluid adsorbed in the rigid pore.

Ustinov and Do[93] included the elastic energy term in the formalism of classical DFT for a LJ fluid in slit pores by minimizing the grand potential of the adsorbed fluid not only with respect to the density profile but also the pore width H. Assuming realistic parameters for microporous carbons, they showed that the elastic response of the pores affects the adsorption isotherms, heats of adsorption and the solvation pressures in the pores only for pores smaller than 1 nm. For pores larger than 1.5 nm, the effects of strain on the adsorption are quite small.

An instructive model has been presented by Guyer and Kim.[126] They considered a model of a cellular solid filled
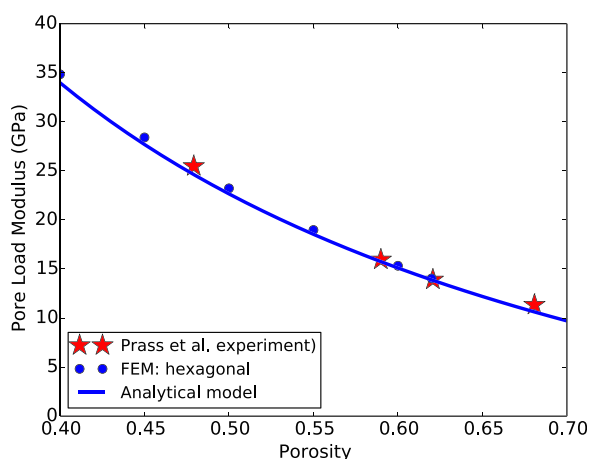

FIG. 20. Pore load modulus of mesoporous silica as a function of porosity. The stars represent the experimental values derived from the experiments by Prass et al.,[65] the circles represent the results of the FEM simulations similar to the one from Ref. 41 and the solid line is the analytical solution Eq. (11). Parameters used for calculations are: $E = 44$ GPa, $\nu = 0.17$.

with fluid, and showed that introduction of coupling between the fluid chemical potential and strain of the solid qualitatively change the process of adsorption and deformation. Although this paper brings an important discussion of the two-way coupling $\epsilon = \epsilon(\mu)$ and $\mu = \mu(\epsilon)$, the predicted results are not supported by any experimental data. Most likely the "emerging hysteresis" predicted by the authors is observable only at very high adsorption-induced strains. At the low strains typically observed in experiments, ϵ of order 10^{-3}, the deformation cannot affect the adsorption isotherm to that extent. In particular, there are a number of systems where adsorption-induced deformation is observed but the isotherms do not show any hysteresis, for example, carbons[37,127] and mesoporous silica with small pore sizes.[30,70] Another work which predicted adsorption-desorption hysteresis due to the flexibility of the adsorbent was a Monte Carlo model by Shen and Siderius.[128] They pointed out that such a model is relevant only to materials with high adsorption strain, such as MOFs.

This idea was further extended by Kulasinski et al.,[129] who considered water sorption on nanoporous biopolymer—amorphous cellulose. This system shows noticeable deformation as well as a change of the elastic constants. Both effects were studied by molecular dynamics simulations and then a coupled thermodynamic-mechanical model was proposed, taking into account the "mechanosorptive effect," i.e., the dependence of the sorption isotherm on mechanical stress. The system considered in Ref. 129 is a soft material, and therefore very different from most of the nanoporous solids discussed in this review. Soft matter behaves in a more complicated fashion compared to a solid. Water sorption causes a change in the material's structure beyond simple elastic deformation, breaking hydrogen bonds between the polymer chains and significantly affecting the elastic properties. In this case, it is absorption rather than adsorption.

The change in elastic constants of porous materials due to adsorption (i.e., non-linear deformation), pointed out in Ref. 129, has been also reported in simulations for conventional non-polymeric porous materials. Using GCMC simulations, Coasne et al. showed that the adsorption of CO_2 in silicalite zeolites causes an increase in the bulk modulus of the framework.[130] A more recent MC simulation study has shown an opposite effect: decrease of the elastic modulus for a slit pore model and for a more complex model representing ELM-11 MOF upon adsorption of LJ fluid.[131] Interestingly, the elastic properties of the *fluids* adsorbed in nanoporous materials also change compared to the bulk fluid. This change was not only shown by Monte Carlo simulations[132] but also measured in ultrasonic experiments.[133,134] In particular, it was shown that the change in the elastic modulus of the adsorbed fluid is linearly related to the adsorption stress in the pores.[135,136]

E. Surface stress approach

The thermodynamic approach to adsorption-induced deformation based on the calculation of adsorption stress or solvation pressure in the fluid confined in the pores discussed in Section III B originates from conventional models of fluid adsorption, where the role of the solid is limited to the attractive potential. Such a representation of a solid is a significant simplification for the consideration of stresses and strains. An alternative way to understand adsorption-induced deformation is based on the concepts of surface science, and is focused on the change of the properties of *the solid surface* upon fluid adsorption. This approach stems from the works of Bangham and coworkers, who concluded that in the course of physisorption on a porous sample, the strain is proportional to the change of the surface energy $\Delta\gamma$ of the material (Eq. (3), "Bangham's law"), see Ref. 7 and references therein.

In the surface science literature, in addition to the surface free energy γ another quantity is introduced—the surface stress f. The surface free energy γ quantifies the work of creating more surface in the undeformed material (e.g., creating a crack or a cavity in a solid) and is related to the breaking of the interatomic bonds. The surface stress f quantifies the work of stretching the existing surface, i.e., stretching the interatomic bonds, without breaking them. This distinction was pointed out as early as in Gibbs' works[137] and has been often revisited in the recent literature.[138–140] A schematic representation shown in Figure 21 illustrates the two cases. In the simple case of isotropic deformation, when the strain ϵ and f are both scalars, surface stress and surface energy are related by the Shuttleworth equation,[141]
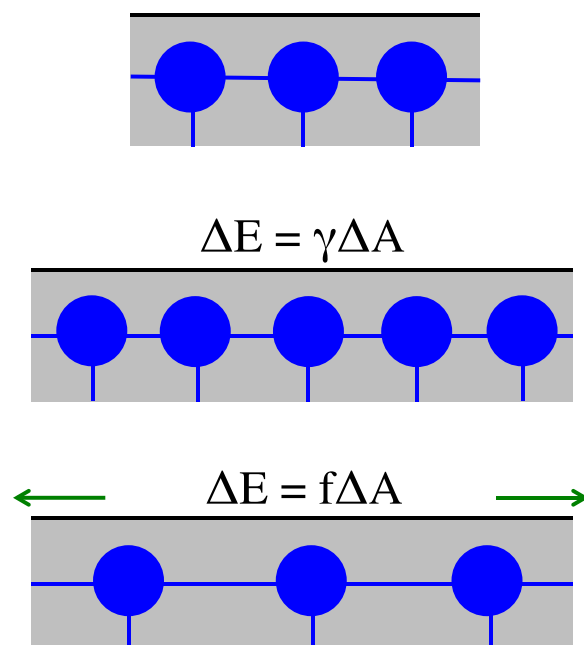

FIG. 21. Illustration of the difference between the surface energy γ and surface stress f for a plane crystalline surface. The blue circles represent the solid atoms, the blue bars represent the interatomic bonds, and the black line represents the solid surface. The top cartoon shows the initial state. The middle cartoon shows the increase of the surface area related to the surface energy, i.e., adding more surface atoms. The bottom cartoon shows the increase of the surface area related to the surface stress, when the number of the surface atoms remains the same, and the area is changing due to stretching the bonds between these atoms. Although for the middle and bottom cartoons the change of the surface area ΔA with respect to the initial state is the same, the energy related to this change could be very different. Reprinted with permission from Gor and Bernstein, Phys. Chem. Chem. Phys. **18**, 9788 (2016). Copyright 2016 Royal Society of Chemistry.

$$f = \gamma + \partial\gamma/\partial\epsilon. \qquad (13)$$

Since adsorption-induced deformation stretches an existing surface, rather than creating new surface, the strain should be related to the *change* of f and not γ. This was pointed out in one of the later works of Bangham.[76] The difference between the change of the surface energy $\Delta\gamma$ and the change of the surface stress Δf with adsorption was first discussed in detail by Eriksson.[142] In the absence of deformation, the change of the surface energy is governed by the Gibbs adsorption equation (2), and in the absence of adsorption, the change of the surface stress is given by the Shuttleworth equation (13). When both effects are present, the Eriksson equation should be used

$$d\gamma = -\Gamma d\mu + (f - \gamma)d\epsilon. \qquad (14)$$

Using the Eriksson equation (14), Halsey considered two different cases of adsorption.[143] The first is an immobile adsorbed lattice gas, so the amount adsorbed is determined not by the surface area (which changes during deformation) but by the number of adsorption sites on this surface (which does not). The second case is mobile adsorption, when the surface area itself determines the amount adsorbed. The strength of adsorption in both cases was expressed as a single parameter k. In both cases, the key contribution to the change of the surface stress with adsorption was related to the dependence of the parameter k on strain.

Recently, two of us developed the ideas of Eriksson and Halsey to put the surface stress approach in the context of adsorption deformation of mesoporous materials.[69] We analyzed the change of the surface stress Δf and the change of the surface energy $\Delta\gamma$ due to adsorption calculated based on the Brunauer-Emmett-Teller (BET) theory.[144] First, we combined Bangham's law and the BET theory by calculating $\Delta\gamma$ based on the BET and predicting deformation based on this quantity. Then we used this approach to predict the adsorption-induced deformation of mesoporous material with channel-like (cylindrical) pores, and compared our predictions to the experimental data of argon and water adsorption on Vycor glass. The comparison showed good agreement; moreover, for argon adsorption on Vycor, a good agreement was also observed with the predictions of the approach based on the calculations of solvation pressure.[80,96]

Then, in addition to the change of the surface energy $\Delta\gamma$, we calculated the change of the surface stress Δf following equations derived in Refs. 142 and 143. We showed that these two values may differ even qualitatively. In our model, the difference between $\Delta\gamma$ and Δf appears when the dependence of the BET constant on strain is taken into account, i.e., in the case of the adsorption-strain coupling. Figure 22 shows Δf as a function of relative gas pressure for the cases of weak (low BET constant) and strong solid-fluid interactions (high BET constant). We show that for both cases Δf can be significantly different from $\Delta\gamma$. We found the condition when the difference between the two vanishes and Bangham's law is applicable: $dE_1/d\epsilon = 0$, where E_1 is the energy of adsorption of the first monolayer of fluid within the BET theory. It is likely that this condition is satisfied in
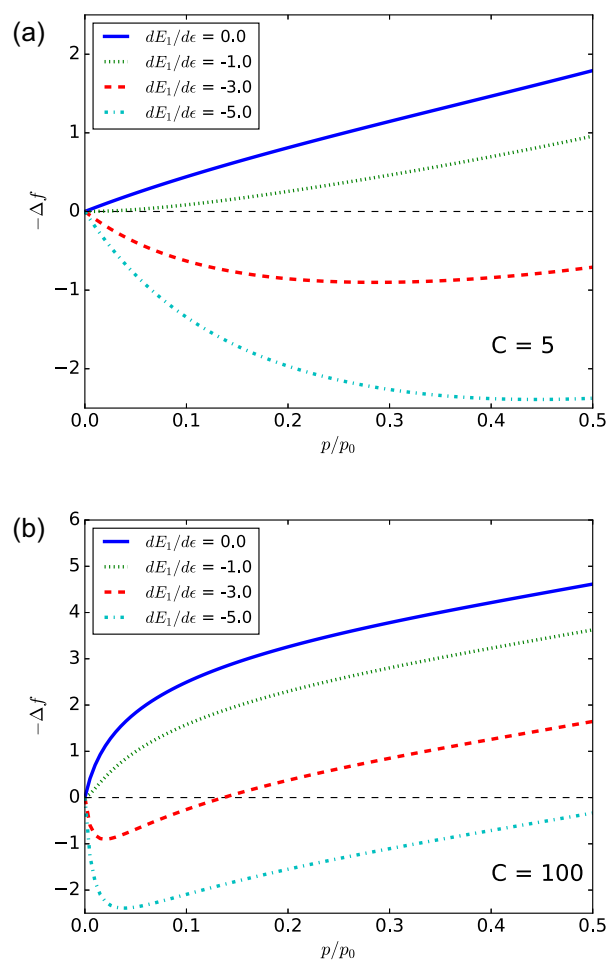
FIG. 22. Reduction of the surface stress $-\Delta f$ (in reduced units) calculated using the extended BET theory, which takes into account the dependence of BET parameters on strain. Top plot shows calculations for low BET constant ($C = 5$) and bottom plot shows calculations for high BET constant ($C = 100$). Different lines correspond to various values of $dE_1/d\epsilon$. $dE_1/d\epsilon = 0$ gives $\Delta f = \Delta\gamma$, i.e., Bangham's law. Reprinted with permission from Gor and Bernstein, Phys. Chem. Chem. Phys. **18**, 9788 (2016). Copyright 2016 Royal Society of Chemistry.

most cases, and that the prediction of strain based on $\Delta\gamma$ is a good approximation, e.g., in the case of argon and water adsorption on Vycor glass. Finally, we showed that the difference between the change of the surface energy $\Delta\gamma$ and the change of the surface stress Δf can explain for the first time some of the experimental data on mesoporous materials that contradicts Bangham's law (see examples in Sections II A and II C for discussion of these experiments).

Another recently developed theory of adsorption-induced deformation based on the change of the surface stress was presented by Rusanov and Kuni,[100] who refer to it as "sorption-striction."[145] Their approach could be considered a hybrid between the solvation pressure approach and surface stress approach: they perform calculations of the pressure tensor in the fluid adsorbed in the pore, and also take into account the change of the surface stress. The latter is calculated based on Eriksson's equation.[142] The pressure tensor calculations were performed for slit, cylindrical, and spherical pore geometries. Assuming the pair potentials to be London dispersion forces (scaling like r^{-6}) or dispersion forces with electromagnetic retardation (scaling like r^{-7}), the

authors obtained analytical expressions for the pressure tensor. Finally, they applied the calculated stress to the stress-strain relations in simple geometries and for the strain normal to the pore walls. According to their derivation, the non-monotonic deformation of micropores often observed in experiments is due to both pressure in the fluid and change of the surface stress. The former is responsible for the initial contraction at low gas pressures and the latter for the following expansion.

While the main focus of the current review is on *porous* materials, it is worth mentioning the calculations of the change of surface stress due to adsorption for *non-porous* materials. An instructive review on the surface stress in non-porous materials and effects of adsorption on it has been given by Haiss.[3] The surface stress has been studied theoretically for a number of systems in which the guest atoms are *chemisorbed* on the surface.[146–149] When adsorbed atoms are chemically bound to the solid surface, the change in surface free energy is dominated by the enthalpy, and the surface stresses can therefore be readily calculated from the electronic structure density functional theory (eDFT) on the static atomic configurations. The first calculation was performed by Feibelman[146] for the effect of H and O adsorption on the stress of the Pt (111) surface, which showed significant reduction of tensile stresses, comparable with experimentally observed data.

eDFT works well for calculations of the surface stress change in the case of chemisorption, when adsorbing atoms become strongly bound to the surface. However, the static eDFT calculation is not sufficient for predicting the change of the surface stress during physisorption of fluid. Fluid molecules can be mobile, and therefore, the change of the surface stress should be estimated from sampling various configurations at non-zero temperature. This can be done, e.g., by performing molecular dynamics simulation. Such simulations using interatomic potentials have been done by Huang an co-workers[150,151] to model adsorption of water on alumina surface. From the predicted change of the surface stress, they estimated the bending of a microcantilever induced by water adsorption.

Recently, two of us carried out calculations of surface stresses for silica surface at room temperature in dry and wet states.[152] In order to avoid the errors related to interatomic potentials for water-silica, we performed *ab initio* molecular dynamics simulations. To reduce the computational costs, we considered a crystalline form of silica—α-quartz. We considered two different quartz surfaces: non-hydroxylated and fully hydroxylated. The resulting *changes* of the surface stresses Δ*f* appeared to be qualitatively different for the two surfaces. For the non-hydroxylated surface, the changes in both surface stress tensor components along the surface are negative, i.e., adsorption causes expansion of the surface in both directions, which is consistent with the Bangham effect. For the hydroxylated surface, we found that while the change of the surface stress in one direction is negative, in the other direction it is positive, i.e., adsorption causes contraction of the surface in this direction. The observation of positive change of the surface stress can qualitatively explain the contraction of mesoporous silica upon water adsorption

experimentally observed recently,[25,38] and the difference in behavior between different hydroxylation levels can explain the variety of behaviors among different experimental observations.[11,25,38,65]

F. Poromechanics approach

The behavior of a porous medium saturated (or partially saturated) with fluid is described within the framework of *poromechanics* or *poroelasticity*, which couples the fluid pressure in the pores with the deformation of the porous medium.[153] Since adsorption-induced deformation falls into this category of phenomena and, moreover, has important applications for geological systems (see Section IV C), there have been several attempts to describe it in terms of poromechanics.

Mushrif and Rey[154] used the equations of linear poroelasticity[153] and expressed the strain of a porous sample as a function of porosity change. The latter was related to the adsorption isotherm and expressed as a function of the difference between the chemical potential of the adsorbate on the strained and unstrained surfaces. The coupling between thermodynamics of adsorption and elasticity of the adsorbent was introduced through the correction of chemical potential, so that the adsorption isotherm was expressed not as $N(\mu)$, but rather as $\mu(N)$. In such a formulation, the chemical potential of the strained surface becomes a function of porosity itself. The authors proposed an iterative scheme to solve the coupled problem and their calculations agreed well with the experimental data on CO_2 adsorption on activated carbon at three different temperatures from Yakovlev *et al.*[155]

Vandamme *et al.*[156] augmented the conventional poromechanics equations with surface stress terms to get predictions of the strain of the porous medium due to the change of the surface stress. In their formulation, it was assumed that the surface stress is changing according to the Gibbs adsorption equation, i.e., in the same way as the surface energy does. The validity of this approximation, however, was not discussed in their paper (see Section III E). To get the change of the surface energy as a function of chemical potential, Vandamme *et al.* used the classical Langmuir adsorption isotherm, which they additionally verified by molecular simulations. Calculations based on their theory for deformation of coal induced by CO_2 and CH_4 adsorption in micropores showed very good agreement with experimental measurements from Ref. 157, see Figure 23. The deformation predicted for mesopores, however, looked very different. Vandamme's group further generalized this approach by including the adsorption isotherms derived from molecular simulations of adsorption in deformable pores,[158] and extended the theory for adsorption of mixtures.[159]

Similar to Vandamme, Pijaudier-Cabot and co-authors proposed an extension of poromechanics for microporous materials.[160] However, the effects of solid-fluid interactions (or "confinement effects" in terms of the authors) were taken into account not through the surface stress, but through the interaction energy ψ_{int} and fluid pressure in the pores, referred to as "interaction" pressure p_{int}. The normal component of the pressure tensor was considered, making it similar
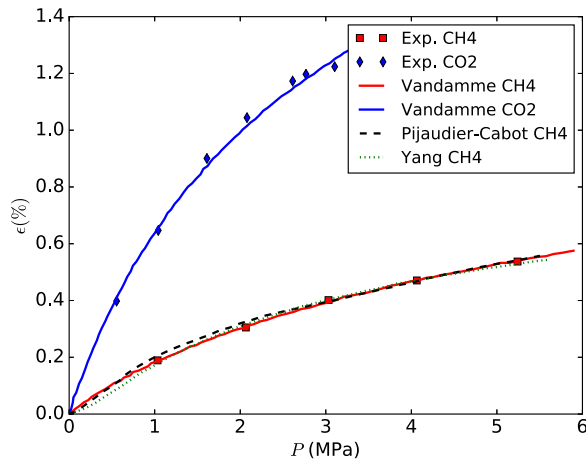
FIG. 23. Adsorption-induced deformation of coal measured experimentally[157] and predicted by three different models: poromechanical models by Vandamme *et al.*[156] and by Pijaudier-Cabot *et al.*,[160] and thermodynamic model by Yang *et al.*[95]

to the Ravikovitch and Neimark approach based on the solvation pressure.[94] The authors emphasize strong dependence of (solvation) pressure on the pore size and introduced the pore size distribution in their formulation. The distribution is accounted for by writing the poromechanics equations in terms of a corrected or an apparent porosity φ^* defined as

$$\varphi^* = \int_{\Omega_0} \rho(R) \frac{\varphi(R)}{\rho_b} \frac{d\Omega_0}{\Omega_0}, \qquad (15)$$

where $\rho(R)$ is the fluid density in the pore with the radius R, ρ_b is the density of the bulk fluid, $\varphi(R)$ is the relative volume of pores (porosity) with radius R, and Ω_0 is the Lagrangian material volume.[161,162] Finally, they proposed a simplified model for practical calculations which assumes that the interaction energy is a function of the apparent porosity only and the interaction pressure is proportional to the surface excess Γ, which is a function of gas pressure p and temperature T

$$p_{int} = -k\Gamma(p, T). \qquad (16)$$

Using k as an adjustable parameter, the authors showed that their model accurately describes the experimental deformation data of CH_4 adsorption on coal from Ref. 157 and on activated carbon from Ref. 163. Since both Vandamme *et al.* and Pijaudier-Cabot *et al.* compared their predictions with the experiments from Ref. 157, it is easy to see that their approaches give essentially the same results (Figure 23).

Since the results from Refs. 160 and 164 predicted noticeable changes of the porosity, Pijaudier-Cabot and co-workers further extended their model to take this change into account.[165] In the extended model, they included two additional effects: (1) change in the elastic properties of a porous material due to the change in the porosity and (2) change in the adsorption isotherms due to the change in the porosity. Including these effects results in a coupled problem of adsorption and deformation. The change of the adsorption isotherms was considered through the change of the pore volume, which is similar to the change of the surface area in

the extended BET model from Ref. 69. A non-trivial change of the adsorption potential was not considered. The authors showed that although the predicted results are close to their initial model,[160,164] unlike the initial model, the extended model is consistent with the observed significant change of the porosity. Note that the theory of Pijaudier-Cabot and co-workers[160,164,165] focuses on microporous materials only and does not give a solution for mesoporous materials.

Unlike the thermodynamic approach of Ravikovitch and Neimark, which assigned the strain of the porous solid fully to the strain of the pore space,[94] poromechanics takes into account that the strain could be both due to the deformation of the pore space and due to the deformation of the pore walls. Yet at small strains this difference may not be too important. This is illustrated by the comparison of predictions of poromechanical models to the predictions of a thermodynamic model for the deformation of coal induced by methane adsorption—the predictions are in excellent agreement. However, this is unlikely to be true if higher strains are considered. For higher strains, when the adsorption process is affected by strain, a model taking into account this coupling is necessary and a poromechanical model could be a viable candidate.

IV. APPLICATIONS OF ADSORPTION-INDUCED DEFORMATION

A. Sensing and actuation

The change of the surface stress due to adsorption and corresponding strains had already found applications as sensing devices in the 1990s.[166–169] All these works, however, involved micro cantilevers, which bend upon change of the surface stress due to adsorption at planar, non-porous surfaces. Stimulated by the significant progress in the experimental and theoretical exploration of adsorption-induced deformation of *porous* materials, a number of groups are attempting to design sensors and actuators for this adsorption geometry. Biener *et al.*[170] studied the change of the surface stress of nanoporous gold upon adsorption of ozone and carbon monoxide, which causes reversible strain. They proposed to use this effect as an actuator. However, nanoporous gold, similar to most nanoporous *solids*, shows very moderate strains of the order of a few tenths of a percent.

Noticeably higher strains can be achieved if a soft nanoporous material is used. A synthesis of a suitable polymer and fabrication of an actuator acting on the adsorption-induced deformation principle was recently proposed by Zhao *et al.*[171] They fabricated a porous polymer membrane, which significantly changed its shape when exposed to water and acetone vapors. Figure 24 (top) shows a photo of the deformation of a porous polymer membrane—placed in acetone vapor (left) and extracted back in air (right). The bottom panel demonstrates reversible opening and closing of a membrane with the change of air humidity.

Since such an actuator is based on adsorption and not absorption, it does not involve slow molecular transport in the polymer itself. The fast transport in the pores and fast adsorption kinetics provides fast response of the actuator. Furthermore, it showed reversibility as well, making it a
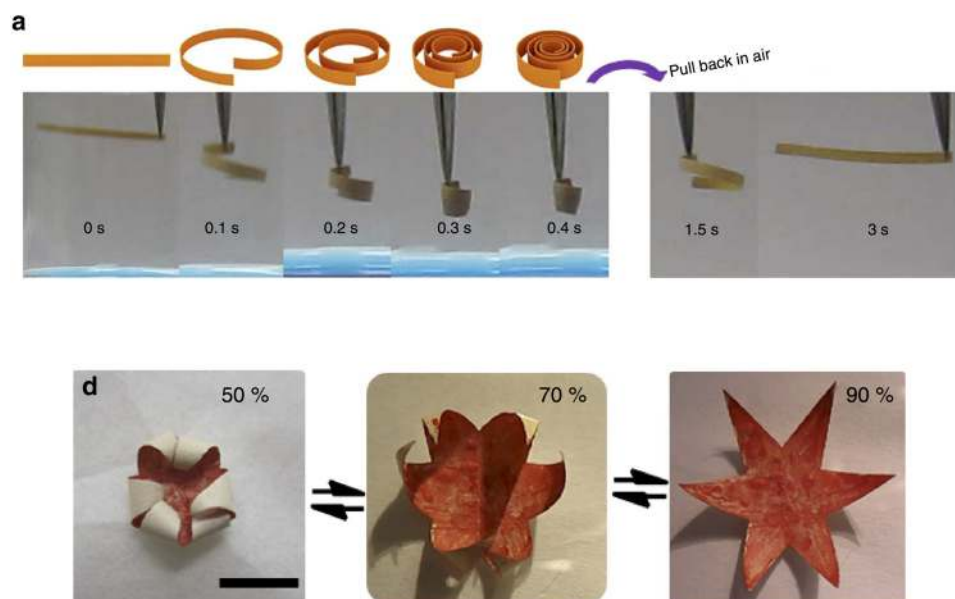
FIG. 24. Top: Adaptive movement of a porous polymer membrane placed in acetone vapor (left) and then back in air (right). Bottom: The reversible opening and closing of a star-shaped membrane actuator "flower" upon switching the air humidity between 50% and 90% at 20 °C. Scale bar 1 cm. Reprinted with permission from Zhao *et al.*, Nat. Commun. **5**, 4293 (2014). Copyright 2014 Nature Publishing Group.

very promising sensing mechanism. More recently, the same team extended the application of these types of actuators to the liquid phase.[172]

Recent literature gives special attention to bio-inspired actuators, and in particular, those that are driven by a change of humidity. Some motivating natural examples are well-known: pine cones, which open and close upon change of air humidity,[173] and humidity-driven propulsion of the dispersal unit of wild wheat.[174] Inspired by the former natural example, Van Opdenbosch and co-authors[175] created an artificial pine cone, made of mesoporous silica, which is able to respond to the change of humidity similarly to the natural one (see Figure 25). Interestingly, the two-dimensional elastic model of adsorption-induced deformation from Ref. 41, described in Section III C, worked satisfactory for that complicated system.

Finally, a significant step toward implementing devices based on adsorption-induced deformation of porous materials has been made by the Paris group.[176] Their idea was based on measuring the deflection of a microcantilever. Since the adsorption capacity of a cantilever's surface is low, they increased the surface area available for adsorption by the deposition of a mesoporous silica film on one side of the cantilever (by dip coating), as shown schematically in Figure 26. In addition to successfully implementing this device, Ganser *et al.* developed a quantitative model of humidity-driven cantilever bending based on the thermodynamic and mechanical theories of adsorption-induced deformation from Refs. 41 and 80. A similar humidity-sensing device has been also recently fabricated by Boudot *et al.*[177]

B. Characterization of porous materials

A straightforward way to employ adsorption-induced deformation is to determine the elastic properties of porous materials from experimental strain isotherms. That was used by Mogilnikov and Baklanov for thin silica films, whose elastic properties are hard to determine using other methods.[23] They calculated the adsorption and strain from ellipsometry data, as described in detail in Refs. 47 and 48, and used the part of the strain isotherm after capillary condensation to get the elastic modulus. As was discussed in Section III B 2, this part of the strain isotherm has a simple logarithmic shape (Eq. (9)) and it is straightforward to extract an elastic constant from it. Despite proposing an elegant method for measuring the elastic response of a thin porous film to the fluid pressure in the pores, Mogilnikov and Baklanov[23] incorrectly interpreted the corresponding elastic constant as "Young's modulus" E_p. Although a relation between the corresponding elastic constant and Young's modulus of the pore walls E or of the porous film E_p can be readily derived, this constant corresponds to a different load and thus should be clearly distinguished. The same misinterpretation also occurs in Ref. 25. Another study on the determination of elastic properties of thin solid films was presented by Dourdain *et al.*[29] Unfortunately, the authors did

FIG. 25. An artificial pine cone made of mesoporous silica is able to mimic the behavior of its natural prototype: adsorption-induced deformation makes the ovuliferous scales of the cone move with the change of humidity. Reprinted with permission from Van Opdenbosch *et al.*, Adv. Mater. **28**, 5235–5240 (2016). Copyright 2016 Wiley.
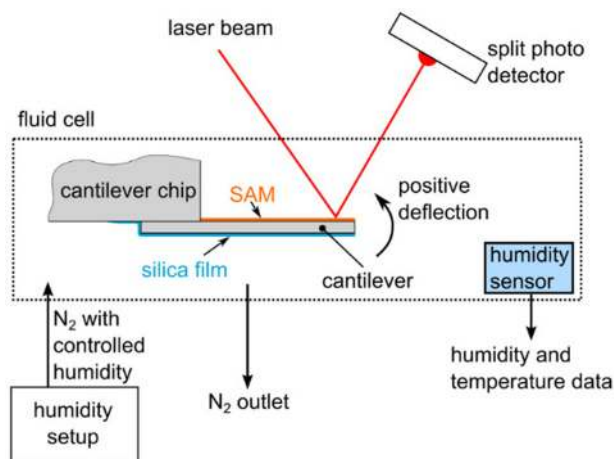
FIG. 26. A cantilever sensor based on adsorption-induced deformation. Deformation of the porous silica film upon water vapor adsorption causes the deflection of the cantilever, measured by the reflection of a laser beam. Reprinted with permission from Ganser *et al.*, Beilstein J. Nanotechnol. **7**, 637 (2016). Copyright 2016 Belstein Publishing.

not specify which elastic constant comes from the effective Hooke's law employed in their analysis.

A different way to use adsorption-induced deformation for materials characterization was proposed by Ustinov and Do.[93] Based on their theoretically predicted strain isotherms, which were very strongly pore-size dependent, they suggested that from experimentally measured strains one can extract information about the pore size distribution (PSD). Recently, Kowalczyk *et al.*[178] reported a combined experimental-modeling study of adsorption-induced deformation of microporous carbon monoliths as an assessment of applicability of *in situ* dilatometry for characterization of microporous materials. It is well-known that nitrogen and argon at cryogenic temperatures are not well suited for characterization of microporous samples.[179] Therefore, in this work the authors used CO_2 at 293 K as an adsorbate. Figure 27 shows the experimental strain (top) and adsorption (bottom) isotherms from Ref. 178. The experimental strain isotherm represents a curve typical of microporous materials: moderate contraction at low pressures (below 10^{-3}) and monotonic expansion at higher pressures. The modeling part of the work constructs a kernel of adsorption isotherms in a series of slit micropores (widths between 0.22 and 2.0 nm) and a corresponding kernel of model strain isotherms, calculated based on the thermodynamic model for "adsorption stress" in the pores $\sigma_a(H,p) = -\frac{1}{A}\frac{\partial \Omega(H,p)}{\partial H}$, where Ω is the grand potential of the pore with the fluid and H is the pore width. The calculation of the kernel is performed by GCMC. The calculated kernel of isotherms is applied for solving the integral adsorption equation to get the PSD using the established procedure.[49] Then, similarly, the kernel of stress isotherms is applied to get the PSD from the strain data, with the elastic modulus as another fitting parameter. The authors conclude that it is constant, i.e., it does not change during the course of adsorption, as discussed in some previous studies.[130,131] The two PSDs, from adsorption isotherm and from strain isotherm, are close. Hence, the authors conclude that the analysis of strain isotherms is a viable approach to
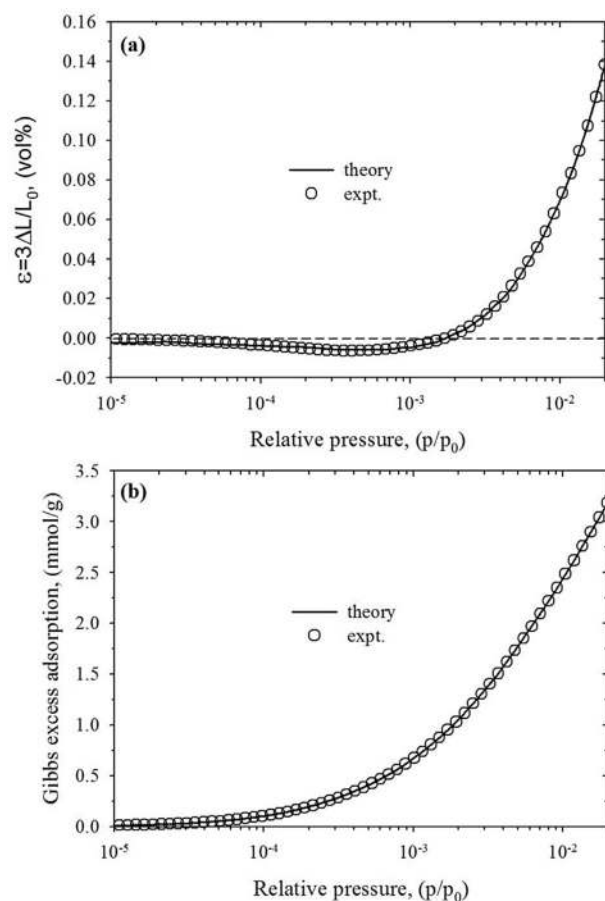

FIG. 27. Adsorption (bottom) and strain (top) isotherms for CO_2 adsorption on carbon monolith at 293 K. Reprinted with permission from Kowalczyk *et al.*, Carbon **103**, 263 (2016). Copyright 2016 Elsevier.

analyze pore-size distributions of microporous carbons. This approach can be used in particular, for the analysis of the smallest pore sizes, several Å wide, for which the adsorption isotherms are indistinguishable.

This idea was further developed by Balzer and co-workers.[50] They employed DFT calculations to derive adsorption and adsorption stress isotherms for carbon micropores and the adsorbates N_2 (77 K), Ar (77 K), and CO_2 (273 K), and compared the results to the experimental data reported earlier.[127] One of the important features of this work was the consideration of micropores smaller than the nominal molecular diameter of the adsorbates, which are typically disregarded. While *adsorption* isotherms for small micropores are quite similar, the isotherm of adsorption-*stress* differs significantly, providing a convenient criterion for characterization. For pores smaller than the nominal molecular diameter of the adsorbates, the adsorption stress is positive (expansive) in the whole range of pressures. For larger micropores, in contrast, it is negative and decreasing at low pressures, reaches a minimum, and then starts to increase and gradually becomes positive for larger pores (contraction-expansion behavior, discussed in Section III A 2).

Analyzing experimental adsorption and adsorption-induced deformation data measured for the same sample with different adsorbates, Balzer *et al.* performed the following analysis. They created DFT kernels for adsorption
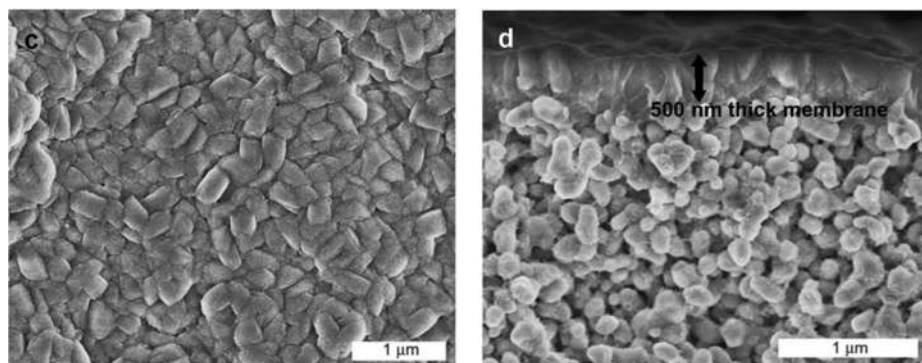
isotherms and adsorption-stress isotherms, then applied the CO_2 kernels to derive the PSD from the experimental CO_2 data. This PSD was quite close to the conventional PSD derived from adsorption data only. Then, they compared the predictions of N_2 and Ar DFT kernels convolved with the obtained PSD to the corresponding adsorption and strain experimental data. The comparison showed reasonable agreement, with significant deviation only at relative pressures below $p/p_0 < 10^{-5}$, proving the viability of PSD calculations based on the adsorption-induced deformation data and its independence from the adsorbed species.

C. Undesired manifestations of adsorption-induced deformation

While for the aforementioned examples (Section IV B) adsorption-induced deformation serves as a tool to get information about the PSD, in other cases this phenomenon can on the contrary complicate the PSD calculations, concealing the "true" PSD. This is the case when the isotherms themselves are strongly affected by the deformation, e.g., in aerogels, which have very high porosity ($\phi > 90\%$) and therefore very low elastic constants. The pore-size distributions obtained from nitrogen adsorption isotherms on aerogels must be corrected for the deformation effects.[17,18]

Another undesired manifestation of adsorption-induced deformation is faced by zeolite membranes. The uniform structure and small size of the zeolites' pores suggest that zeolites could be applied as separation membrane materials. In the last two decades, substantial progress towards this goal has been made, so that to date some of the zeolite membranes are already used on industrial scale.[180,181] Zeolite membranes are synthesized by introducing *ex situ* prepared crystal seeds on a porous substrate and further *in situ* growth of the zeolite layer.[181] This procedure leads to the formation of a structure composed of multiple micrometer sized crystallites (Figure 28). This composite structure inevitably has numerous defects–most prominently intercrystalline spaces, which are larger than the zeolite pores. A thorough characterization of the zeolite membranes showed that these defects can noticeably contribute to the zeolite membrane transport.[182] Moreover, recent *in situ* X-ray diffraction and optical microscopy studies have shown that adsorption of molecules in the zeolite pores causes the swelling of the crystallites and change of the defects sizes in the membranes (Figure 29).[183] This effect alters the permeation and separation properties of

the membranes, so that the membrane transport fails to obey the Maxwell-Stefan law.[184] A detailed review on adsorption-induced deformation of zeolite membranes has recently been presented by Ilić and Wettstein.[185]

Drying of cement and concrete is accompanied with shrinkage, and this effect is another manifestation of adsorption-induced deformation (or *desorption* in the case of drying). This phenomenon was recently discussed in a review by Scherer,[186] and can be described as follows. When Portland cement is hydrated, it forms a nanoporous gel, with mesopores in particular. Equilibrium drying of such material is governed by fluid desorption from mesopores, discussed above in Section III B 2, i.e., a joint action of capillary forces and disjoining pressure, yet the resulting impact strongly depends on kinetics.[186] In any case, drying of cement paste results in its shrinkage that causes microcracking of cementitious materials, which causes great practical concern.

The ability to deform upon adsorption is an intrinsic property of any porous materials, therefore it is not limited to man-made materials, but is observed in natural materials also. Early experiments showed that upon adsorption of methane or carbon dioxide coal can expand[8] or contract.[187] The expansion ("swelling") of coal due to adsorption plays a crucial role for recovery of coal-bed methane. Significant amount of coal-bed methane is present in the adsorbed state in the coal pores.[188,189] In order to extract the adsorbed methane (enhanced coal-bed methane recovery or ECBMR), carbon dioxide is injected into the formation. Since the coal-CO_2 molecular attraction is stronger than coal-CH_4, CO_2 displaces methane. As a result, methane becomes extracted (desorbed) from pores, while CO_2 is adsorbed. However, stronger intermolecular forces cause stronger adsorption-
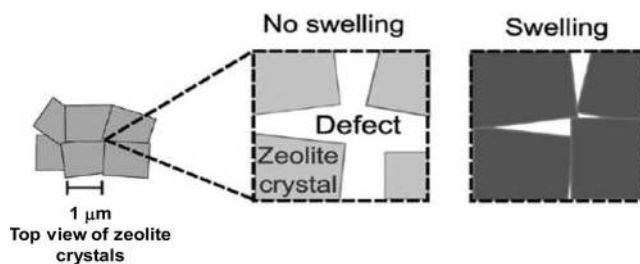

FIG. 29. Schematic of adsorption-induced swelling of zeolite crystallites and consequent effect on the defects. Reprinted with permission from Yu *et al.*, Acc. Chem. Res. **44**, 1196 (2011). Copyright 2011 American Chemical Society.

induced deformation effects, i.e., higher strains. Swelling results in the narrowing and even closing of the macropores and fractures that are providing the permeability of the coal formation, complicating the ECBMR operation. Substantial amounts of work have been done in an attempt to develop models for adsorption-induced coal swelling in the last decade,[158,190–196] yet it still remains a challenging problem. Moreover, there is a concern that adsorption-induced deformation may affect the extraction of shale gas in a way similar to ECBMR.[197]

V. SUMMARY AND OUTLOOK

In recent years, there has been significant progress in experimental measurements and theoretical modeling of adsorption-induced deformation of porous materials. Moreover, this progress has brought the research of adsorption-induced deformation from the purely fundamental to a rather applied realm, so that in particular, fabrication of sensors based on this phenomenon has become realistic. Nevertheless, a number of both fundamental and applied questions remained unanswered. In our understanding, solving the following problems will drive the further development of our knowledge about this peculiar phenomenon.

- Performing reliable measurements of adsorption-induced strains in more than one direction.
- Getting the elastic modulus of porous materials, independent of the adsorption-induced strains measurements, to provide quantitative verification of the models and develop the characterization methods with respect to elastic properties.
- Developing methods for measuring adsorption-induced deformation of powders, since many porous materials cannot be synthesized as monoliths.
- Developing a coupled theory of adsorption-deformation, taking into account change of the adsorption potential (or enthalpy of adsorption) due to strain, which can be verified experimentally.
- Developing a theory of adsorption-induced deformation of soft materials, where the strains can reach tens of percents. Such theory has to take into account the change of the pore size distribution due to the strains induced during adsorption.
- Including the pore size distribution and geometrical distribution of pores in the model for adsorption-deformation. While a homogeneous model[108] could work for highly disordered materials, it cannot describe materials where the micropores and mesopores are distributed in a certain well-defined fashion (e.g., SBA-15, in which the mesopores are believed to have a microporous corona around them).
- Developing quantitative models for non-trivial strain isotherms, e.g., for mesoporous materials, which exhibit contraction at low pressures.
- Developing a theoretical framework for application of experimentally measured strain isotherms to calculate pore size distributions. This requires, in particular, calculation of well-calibrated kernels of adsorption-induced

strain isotherms, similar to those for calculating PSD from adsorption data.[49]
- Fabrication of an adsorption-induced deformation sensing device with a reasonably high resolution, e.g. based on the prototype proposed in Ref. 175.

[1] J. Rouquerol, F. Rouquerol, P. Llewellyn, G. Maurin, and K. S. Sing, *Adsorption by Powders and Porous Solids: Principles, Methodology and Applications* (Academic Press, 2013).
[2] M. Thommes, K. Kaneko, A. V. Neimark, J. P. Olivier, F. Rodriguez-Reinoso, J. Rouquerol, and K. S. W. Sing, Pure Appl. Chem. **87**, 1051 (2015).
[3] W. Haiss, Rep. Prog. Phys. **64**, 591 (2001).
[4] J. W. McBain and J. Ferguson, J. Phys. Chem. **31**, 564 (1927).
[5] F. T. Meehan, Proc. R. Soc. London, Ser. A **115**, 199 (1927).
[6] D. H. Bangham and N. Fakhoury, Nature **122**, 681 (1928).
[7] D. H. Bangham and R. I. Razouk, Proc. R. Soc. London, Ser. A **166**, 572 (1938).
[8] H. Briggs and R. Sinha, Proc. R. Soc. Edinburgh **53**, 48 (1934).
[9] R. S. Haines and R. McIntosh, J. Chem. Phys. **15**, 28 (1947).
[10] M. Lakhanpal and E. Flood, Can. J. Chem. **35**, 887 (1957).
[11] C. H. Amberg and R. McIntosh, Can. J. Chem. **30**, 1012 (1952).
[12] B. Bering, O. Krasil'nikova, A. Sarakhov, V. Serpinskii, and M. Dubinin, Russ. Chem. Bull. **26**, 2258 (1977).
[13] B. Mentzen and P. Gelin, Mater. Res. Bull. **30**, 373 (1995).
[14] H. Van Koningsveld and J. Jansen, Microporous Mater. **6**, 159 (1996).
[15] G. Dolino, D. Bellet, and C. Faivre, Phys. Rev. B **54**, 17919 (1996).
[16] H. Van Koningsveld and J. Koegler, Microporous Mater. **9**, 71 (1997).
[17] G. Reichenauer and G. W. Scherer, J. Non-Cryst. Solids **277**, 162 (2000).
[18] G. Reichenauer and G. W. Scherer, J. Non-Cryst. Solids **285**, 167 (2001).
[19] G. Reichenauer and G. W. Scherer, Colloids Surf., A **187**, 41 (2001).
[20] S. Nair and M. Tsapatsis, J. Phys. Chem. B **104**, 8982 (2000).
[21] Y. Lee, T. Vogt, J. A. Hriljac, J. B. Parise, and G. Artioli, J. Am. Chem. Soc. **124**, 5466 (2002).
[22] P.-A. Albouy and A. Ayral, Chem. Mater. **14**, 3391 (2002).
[23] K. P. Mogilnikov and M. R. Baklanov, Electrochem. Solid-State Lett. **5**, F29 (2002).
[24] C. Serre, F. Millange, C. Thouvenot, M. Noguès, G. Marsolier, D. Louër, and G. Férey, J. Am. Chem. Soc. **124**, 13519 (2002).
[25] C. Boissiere, D. Grosso, S. Lepoutre, L. Nicole, A. B. Bruneau, and C. Sanchez, Langmuir **21**, 12362 (2005).
[26] T. Herman, J. Day, and J. Beamish, Phys. Rev. B **73**, 094127 (2006).
[27] G. A. Zickler, S. Jähnert, S. S. Funari, G. H. Findenegg, and O. Paris, J. Appl. Crystallogr. **40**, s522 (2007).
[28] C. Serre, S. Bourrelly, A. Vimont, N. A. Ramsahye, G. Maurin, P. L. Llewellyn, M. Daturi, Y. Filinchuk, O. Leynaud, P. Barnes *et al.*, Adv. Mater. **19**, 2246 (2007).
[29] S. Dourdain, D. Britton, H. Reichert, and A. Gibaud, Appl. Phys. Lett. **93**, 183108 (2008).
[30] G. Günther, J. Prass, O. Paris, and M. Schoen, Phys. Rev. Lett. **101**, 086104 (2008).
[31] J. B. Lee, H. H. Funke, R. D. Noble, and J. L. Falconer, J. Membr. Sci. **321**, 309 (2008).
[32] S. G. Sorenson, J. R. Smyth, M. Kocirik, A. Zikanova, R. D. Noble, and J. L. Falconer, Ind. Eng. Chem. Res. **47**, 9611 (2008).
[33] J. B. Lee, H. H. Funke, R. D. Noble, and J. L. Falconer, J. Membr. Sci. **341**, 238 (2009).
[34] S. G. Sorenson, E. A. Payzant, W. T. Gibbons, B. Soydas, H. Kita, R. D. Noble, and J. L. Falconer, J. Membr. Sci. **366**, 413 (2011).
[35] M. P. Rossi, Y. Gogotsi, and K. G. Kornev, Langmuir **25**, 2804 (2009).

[36]L.-H. Shao, H.-J. Jin, R. N. Viswanath, and J. Weissmüller, Europhys. Lett. **89**, 66001 (2010).

[37]C. Balzer, T. Wildhage, S. Braxmeier, G. Reichenauer, and J. P. Olivier, Langmuir **27**, 2553 (2011).

[38]P. Sharifi, B. Marmiroli, B. Sartori, F. Cacho-Nerin, J. Keckes, H. Amenitsch, and O. Paris, Bioinspired, Biomimetic Nanobiomater. **3**, 183 (2014).

[39]K. Schappert and R. Pelster, Langmuir **30**, 14004 (2014).

[40]A. Grosman, J. Puibasset, and E. Rolley, Europhys. Lett. **109**, 56002 (2015).

[41]G. Y. Gor, L. Bertinetti, N. Bernstein, T. Hofmann, P. Fratzl, and P. Huber, Appl. Phys. Lett. **106**, 261901 (2015).

[42]J. Bahadur, Y. B. Melnichenko, L. He, C. I. Contescu, N. C. Gallego, and J. R. Carmichael, Carbon **95**, 535 (2015).

[43]C. Balzer, R. Morak, M. Erko, C. Triantafillidis, N. Hüsing, G. Reichenauer, and O. Paris, Z. Phys. Chem. **229**, 1189–1209 (2015).

[44]O. Krasil'nikova, B. Bering, V. Serpinskii, and M. Dubinin, Russ. Chem. Bull. **26**, 1099 (1977).

[45]B. Bering, O. Krasil'nikova, and V. Serpinskii, Russ. Chem. Bull. **27**, 2515 (1978).

[46]T. Hofmann, D. Wallacher, R. Toft-Petersen, B. Ryll, M. Reehuis, and K. Habicht, "Phonons in mesoporous silicon: The influence of nanostructuring on the dispersion in the Debye regime," Micropor. Mesopor. Mat. (published online).

[47]F. N. Dultsev and M. R. Baklanov, Electrochem. Solid-State Lett. **2**, 192 (1999).

[48]M. R. Baklanov, K. P. Mogilnikov, V. G. Polovinkin, and F. N. Dultsev, J. Vac. Sci. Technol., B **18**, 1385 (2000).

[49]J. Landers, G. Y. Gor, and A. V. Neimark, Colloids Surf., A **437**, 3 (2013).

[50]C. Balzer, R. T. Cimino, G. Y. Gor, A. V. Neimark, and G. Reichenauer, Langmuir **32**, 8265 (2016).

[51]C. T. Kresge, M. E. Leonowicz, W. J. Roth, J. C. Vartuli, and J. S. Beck, Nature **359**, 710 (1992).

[52]J. S. Beck, J. C. Vartuli, W. J. Roth, M. E. Leonowicz, C. T. Kresge, K. D. Schmitt, C. T. W. Chu, D. H. Olson, and E. W. Sheppard, J. Am. Chem. Soc. **114**, 10834 (1992).

[53]D. Zhao, J. Feng, Q. Huo, N. Melosh, G. H. Fredrickson, B. F. Chmelka, and G. D. Stucky, Science **279**, 548 (1998).

[54]D. Zhao, Q. Huo, J. Feng, B. F. Chmelka, and G. D. Stucky, J. Am. Chem. Soc. **120**, 6024 (1998).

[55]M. Imperor-Clerc, P. Davidson, and A. Davidson, J. Am. Chem. Soc. **122**, 11925 (2000).

[56]T. Hofmann, D. Wallacher, P. Huber, R. Birringer, K. Knorr, A. Schreiber, and G. Findenegg, Phys. Rev. B **72**, 064122 (2005).

[57]G. A. Zickler, S. Jähnert, W. Wagermaier, S. S. Funari, G. H. Findenegg, and O. Paris, Phys. Rev. B **73**, 184109 (2006).

[58]K. J. Alvine, O. G. Shpyrko, P. S. Pershan, K. Shin, and T. P. Russell, Phys. Rev. Lett. **97**, 175503 (2006).

[59]C. J. Gommes, Langmuir **28**, 5101 (2012).

[60]T. Hofmann, D. Wallacher, J. Perlich, S. K. Vayalil, and P. Huber, Langmuir **32**, 2928 (2016).

[61]Z. Tun, P. Mason, F. Mansour, and H. Peemoeller, Langmuir **18**, 975 (2002).

[62]E. Hoinkis, Part. Part. Syst. Charact. **21**, 80 (2004).

[63]Y. B. Melnichenko, G. D. Wignall, D. R. Cole, and H. Frielinghaus, J. Chem. Phys. **124**, 204711 (2006).

[64]C. Schaefer, T. Hofmann, D. Wallacher, P. Huber, and K. Knorr, Phys. Rev. Lett. **100**, 175701 (2008).

[65]J. Prass, D. Müter, P. Fratzl, and O. Paris, Appl. Phys. Lett. **95**, 083121 (2009).

[66]J. Prass, D. Müter, M. Erko, and O. Paris, J. Appl. Crystallogr. **45**, 798 (2012).

[67]S. Krause, V. Bon, I. Senkovska, U. Stoeck, D. Wallacher, D. M. Többens, S. Zander, R. S. Pillai, G. Maurin, F.-X. Coudert *et al.*, Nature **532**, 348 (2016).

[68]H. S. Cho, H. Deng, K. Miyasaka, Z. Dong, M. Cho, A. V. Neimark, J. K. Kang, O. M. Yaghi, and O. Terasaki, Nature **527**, 503 (2015).

[69]G. Y. Gor and N. Bernstein, Phys. Chem. Chem. Phys. **18**, 9788 (2016).

[70]G. Y. Gor, O. Paris, J. Prass, P. A. Russo, M. M. L. Ribeiro Carrott, and A. V. Neimark, Langmuir **29**, 8601 (2013).

[71]D. H. Bangham and N. Fakhoury, Proc. R. Soc. London, Ser. A **130**, 81 (1930).

[72]D. H. Bangham, N. Fakhoury, and A. F. Mohamed, Proc. R. Soc. London, Ser. A **138**, 162 (1932).

[73]D. H. Bangham, N. Fakhoury, and A. F. Mohamed, Proc. R. Soc. London, Ser. A **147**, 152 (1934).

[74]D. H. Bangham, Proc. R. Soc. London, Ser. A **147**, 175 (1934).

[75]In this approach, we attribute all the changes related to the adsorption to the surface energy of the solid surface $\gamma(\Gamma)$. In Section III B 2, we follow an alternative approach of Derjaguin, in which the surface energy of the solid remains constant γ_s and an additional term is changing with adsorption—disjoining pressure $\Pi(\Gamma)$.

[76]D. H. Bangham, Trans. Faraday Soc. **33**, 805 (1937).

[77]E. O. Wiig and A. Juhola, J. Am. Chem. Soc. **71**, 561 (1949).

[78]D. Yates, J. Phys. Chem. **60**, 543 (1956).

[79]S. G. Ash, D. H. Everett, and C. Radke, J. Chem. Soc. Faraday Trans. II **69**, 1256 (1973).

[80]G. Y. Gor and A. V. Neimark, Langmuir **26**, 13021 (2010).

[81]J. Shen and P. A. Monson, Mol. Phys. **100**, 2031 (2002).

[82]D. Do, D. Nicholson, and H. Do, J. Phys. Chem. C **112**, 14075 (2008).

[83]M. Schoen, O. Paris, G. Günther, D. Müter, J. Prass, and P. Fratzl, Phys. Chem. Chem. Phys. **12**, 11267 (2010).

[84]M. Schoen and G. Günther, Soft Matter **6**, 5832 (2010).

[85]P. Kowalczyk, S. Furmaniak, P. A. Gauden, and A. P. Terzyk, J. Phys. Chem. C **114**, 5126 (2010).

[86]S. Abaza, G. L. Aranovich, and M. D. Donohue, Mol. Phys. **110**, 1289 (2012).

[87]P. Kowalczyk, S. Furmaniak, P. A. Gauden, and A. P. Terzyk, J. Phys. Chem. C **116**, 1740 (2012).

[88]V. T. Nguyen, D. Do, and D. Nicholson, J. Colloid Interface Sci. **388**, 209 (2012).

[89]C. Triguero, F.-X. Coudert, A. Boutin, A. H. Fuchs, and A. V. Neimark, J. Chem. Phys. **137**, 184702 (2012).

[90]F.-X. Coudert, A. Boutin, A. H. Fuchs, and A. V. Neimark, J. Phys. Chem. Lett. **4**, 3198 (2013).

[91]J. E. Santander, M. Tsapatsis, and S. M. Auerbach, Langmuir **29**, 4866 (2013).

[92]R. Diao, C. Fan, D. D. Do, and D. Nicholson, J. Phys. Chem. C **120**, 29272–29282 (2016).

[93]E. Ustinov and D. Do, Carbon **44**, 2652 (2006).

[94]P. I. Ravikovitch and A. V. Neimark, Langmuir **22**, 10864 (2006).

[95]K. Yang, X. Lu, Y. Lin, and A. V. Neimark, Energy Fuels **24**, 5955 (2010).

[96]G. Y. Gor and A. V. Neimark, Langmuir **27**, 6926 (2011).

[97]T. S. Jakubov and D. E. Mainwaring, Phys. Chem. Chem. Phys. **4**, 5678 (2002).

[98]P. Dergunov, A. Klinger, A. Tvardovskii, and A. Fomkin, J. Eng. Phys. Thermophys. **79**, 276 (2006).

[99]A. I. Rusanov, Dokl. Phys. Chem. **406**, 49 (2006).

[100]A. I. Rusanov and F. M. Kuni, Russ. J. Gen. Chem. **77**, 371 (2007).

[101]A. V. Neimark, F.-X. Coudert, A. Boutin, and A. H. Fuchs, J. Phys. Chem. Lett. **1**, 445 (2010).

[102]B. P. Bering and V. V. Serpinskii, Bull. Acad. Sci. USSR, Div. Chem. Sci. **22**, 2616 (1973).

[103]"Vacancy solution theory" treats the fluid adsorbed in a pore as a mixture of fluids atoms and virtual particles representing vacancies, and applies solution thermodynamics to describe its properties. Using this formalism, Jakubov and Mainwaring predicted the pressure in the pores and employed Hooke's law to calculate the strain.

[104]P. I. Ravikovitch and A. V. Neimark, Langmuir **18**, 1550 (2002).

[105]J. E. Curry, F. Zhang, J. H. Cushman, M. Schoen, and D. J. Diestler, J. Chem. Phys. **101**, 10824 (1994).

[106]E. N. Brodskaya, A. I. Rusanov, and F. M. Kuni, Colloid J. **72**, 602 (2010).

[107]Y. Long, J. C. Palmer, B. Coasne, M. Śliwinska-Bartkowiak, and K. E. Gubbins, Microporous Mesoporous Mater. **154**, 19 (2012).

[108]P. Kowalczyk, A. Ciach, and A. V. Neimark, Langmuir **24**, 6603 (2008).

[109]K. Yang, X. Lu, Y. Lin, and A. V. Neimark, J. Geophys. Res., B: Solid Earth **116**, B08212 (2011).

[110]A. V. Neimark and P. I. Ravikovitch, Microporous Mesoporous Mater. **44**, 697 (2001).

[111]T. Horikawa, D. D. Do, and D. Nicholson, Adv. Colloid Interface Sci. **169**, 40 (2011).

[112]P. Monson, Microporous Mesoporous Mater. **160**, 47 (2012).

[113]B. V. Derjaguin, Acta Physicochim. URSS **12**, 181 (1940).

[114]J. Broekhoff and J. De Boer, J. Catal. **9**, 8 (1967).

[115]P. I. Ravikovitch and A. V. Neimark, Langmuir **22**, 11171 (2006).

[116]S. Jähnert, D. Müter, J. Prass, G. A. Zickler, O. Paris, and G. H. Findenegg, J. Phys. Chem. C **113**, 15201 (2009).

[117]B. V. Derjaguin, N. V. Churaev, and V. M. Muller, *Surface Forces* (Consultants Bureau, New York, 1987).

[118]A. Frumkin, Zh. Fiz. Khim. **12**, 337 (1938).

[119]D. Bangham and F. Maggs, *The Strength and Elastic Constants of Coals in Relation to Their Ultra-Fine Structure* (The British Coal Utilisation Research Association, The Royal Institution, London, 1944), pp. 118–130.

[120]D. Yates, Proc. Phys. Soc. London, Sect. B **65**, 80 (1952).

[121]G. W. Scherer, J. Am. Ceram. Soc. **69**, 473 (1986).

[122]L. J. Gibson and M. F. Ashby, Proc. R. Soc. London, Ser. A **382**, 43 (1982).

[123]L. J. Gibson and M. F. Ashby, *Cellular Solids: Structure and Properties* (Cambridge University Press, 1999).

[124]M. Liu, J. Wu, Y. Gan, and C. Q. Chen, AIP Adv. **6**, 035324 (2016).

[125]M. Liu, Y. Zhang, J. Wu, Y. Gan, and C. Chen, Int. J. Eng. Sci. **107**, 68 (2016).

[126]R. A. Guyer and H. A. Kim, Phys. Rev. E **91**, 042406 (2015).

[127]C. Balzer, S. Braxmeier, A. V. Neimark, and G. Reichenauer, Langmuir **31**, 12512 (2015).

[128]V. K. Shen and D. W. Siderius, J. Chem. Phys. **140**, 244106 (2014).

[129]K. Kulasinski, R. Guyer, D. Derome, and J. Carmeliet, Phys. Rev. E **92**, 022605 (2015).

[130]B. Coasne, J. Haines, C. Levelut, O. Cambon, M. Santoro, F. Gorelli, and G. Garbarino, Phys. Chem. Chem. Phys. **13**, 20096 (2011).

[131]F. Mouhat, D. Bousquet, A. Boutin, L. B. du Bourg, F.-X. Coudert, and A. H. Fuchs, J. Phys. Chem. Lett. **6**, 4265 (2015).

[132]G. Y. Gor, D. W. Siderius, C. J. Rasmussen, W. P. Krekelberg, V. K. Shen, and N. Bernstein, J. Chem. Phys. **143**, 194506 (2015).

[133]J. H. Page, J. Liu, B. Abeles, E. Herbolzheimer, H. W. Deckman, and D. A. Weitz, Phys. Rev. E **52**, 2763 (1995).

[134]K. Schappert and R. Pelster, Europhys. Lett. **105**, 56001 (2014).

[135]G. Y. Gor, Langmuir **30**, 13564 (2014).

[136]G. Y. Gor, D. W. Siderius, V. K. Shen, and N. Bernstein, J. Chem. Phys. **145**, 164505 (2016).

[137]J. W. Gibbs, *The Scientific Papers of J. Willard Gibbs* (Longmans, Green and Company, 1906), Vol. 1.

[138]R. C. Cammarata and K. Sieradzki, Annu. Rev. Mater. Sci. **24**, 215 (1994).

[139]A. I. Rusanov, Surf. Sci. Rep. **58**, 111 (2005).

[140]D. Kramer and J. Weissmüller, Surf. Sci. **601**, 3042 (2007).

[141]R. Shuttleworth, Proc. Phys. Soc. London, Sect. A **63**, 444 (1950).

[142]J. C. Eriksson, Surf. Sci. **14**, 221 (1969).

[143]G. Halsey, Surf. Sci. **72**, 1 (1978).

[144]S. Brunauer, P. H. Emmett, and E. Teller, J. Am. Chem. Soc. **60**, 309 (1938).

[145]Rusanov uses the term "mechanical surface tension" for the surface stress and "thermodynamic surface tension" for the surface energy.

[146]P. J. Feibelman, Phys. Rev. B **56**, 2175 (1997).

[147]M. J. Harrison, D. Woodruff, and J. Robinson, Surf. Sci. **602**, 226 (2008).

[148]Z. Tian, D. Sander, N. N. Negulyaev, V. S. Stepanyuk, and J. Kirschner, Phys. Rev. B **81**, 113407 (2010).

[149]M. K. Bradley, D. Woodruff, J. Robinson, D. C. Sheppard, and A. Hentz, Surf. Sci. **635**, 27 (2015).

[150]H. Yu, Q.-A. Huang, and X.-X. Liu, Appl. Surf. Sci. **255**, 9404 (2009).

[151]B. Li and Q.-A. Huang, Appl. Surf. Sci. **282**, 662 (2013).

[152]G. Y. Gor and N. Bernstein, Langmuir **32**, 5259 (2016).

[153]O. Coussy, *Poromechanics* (John Wiley & Sons, 2004).

[154]S. H. Mushrif and A. D. Rey, Chem. Eng. Sci. **64**, 4744 (2009).

[155]V. Y. Yakovlev, A. A. Fomkin, A. V. Tvardovskii, and V. A. Sinitsyn, Russ. Chem. Bull. **54**, 1373 (2005).

[156]M. Vandamme, L. Brochard, B. Lecampion, and O. Coussy, J. Mech. Phys. Solids **58**, 1489 (2010).

[157]J. R. Levine, Geol. Soc., London, Spec. Publ. **109**, 197 (1996).

[158]L. Brochard, M. Vandamme, and R.-M. Pellenq, J. Mech. Phys. Solids **60**, 606 (2012).

[159]S. Nikoosokhan, M. Vandamme, and P. Dangla, J. Mech. Phys. Solids **71**, 97–111 (2014).

[160]G. Pijaudier-Cabot, R. Vermorel, C. Miqueu, and B. Mendiboure, C. R. Méc. **339**, 770 (2011).

[161]Lagrangian volume is related to the same material points. In contrast to the steady Eulerian volume, the amount of mass in the moving Lagrangian volume remains constant, but the dimensions of the volume may change due to the internal expansion/contraction processes.

[162]T. Gerya, *Introduction to Numerical Geodynamic Modelling* (Cambridge University Press, 2009).

[163]A. Knorst-Fouran, Ph.D. thesis, Université de Pau et des Pays de l'Adour, 2010.

[164]R. Vermorel and G. Pijaudier-Cabot, Eur. J. Mech., A **44**, 148 (2014).

[165]L. Perrier, G. Pijaudier-Cabot, and D. Grégoire, Continuum Mech. Thermodyn. **27**, 195 (2015).

[166]G. Y. Chen, T. Thundat, E. A. Wachter, and R. J. Warmack, J. Appl. Phys. **77**, 3618 (1995).

[167]H.-J. Butt, J. Colloid Interface Sci. **180**, 251 (1996).

[168]T. Thundat, P. I. Oden, and R. J. Warmack, Microscale Thermophys. Eng. **1**, 185 (1997).

[169]R. Berger, E. Delamarche, H. P. Lang, C. Gerber, J. K. Gimzewski, E. Meyer, and H.-J. Güntherodt, Science **276**, 2021 (1997).

[170]J. Biener, A. Wittstock, L. Zepeda-Ruiz, M. Biener, V. Zielasek, D. Kramer, R. Viswanath, J. Weissmüller, M. Bäumer, and A. Hamza, Nat. Mater. **8**, 47 (2009).

[171]Q. Zhao, J. W. Dunlop, X. Qiu, F. Huang, Z. Zhang, J. Heyda, J. Dzubiella, M. Antonietti, and J. Yuan, Nat. Commun. **5**, 4293 (2014).

[172]Q. Zhao, J. Heyda, J. Dzubiella, K. Täuber, J. W. Dunlop, and J. Yuan, Adv. Mater. **27**, 2913 (2015).

[173]L. Bertinetti, F. Fischer, and P. Fratzl, Phys. Rev. Lett. **111**, 238001 (2013).

[174]R. Elbaum, L. Zaltzman, I. Burgert, and P. Fratzl, Science **316**, 884 (2007).

[175]D. Van Opdenbosch, G. Fritz-Popovski, W. Wagermaier, O. Paris, and C. Zollfrank, Adv. Mater. **28**, 5235–5240 (2016).

[176]C. Ganser, G. Fritz-Popovski, R. Morak, P. Sharifi, B. Marmiroli, B. Sartori, H. Amenitsch, T. Griesser, C. Teichert, and O. Paris, Beilstein J. Nanotechnol. **7**, 637 (2016).

[177]M. Boudot, H. Elettro, and D. Grosso, ACS Nano **10**, 10031 (2016).

[178]P. Kowalczyk, C. Balzer, G. Reichenauer, A. P. Terzyk, P. A. Gauden, and A. V. Neimark, Carbon **103**, 263 (2016).

[179]M. Thommes and K. A. Cychosz, Adsorption **20**, 233 (2014).

[180]J. Gascon, F. Kapteijn, B. Zornoza, V. Sebastián, C. Casado, and J. Coronas, Chem. Mater. **24**, 2829 (2012).

[181]N. Rangnekar, N. Mittal, B. Elyassi, J. Caro, and M. Tsapatsis, Chem. Soc. Rev. **44**, 7128 (2015).

[182]M. Yu, R. D. Noble, and J. L. Falconer, Acc. Chem. Res. **44**, 1196 (2011).

[183]S. G. Sorenson, J. R. Smyth, R. D. Noble, and J. L. Falconer, Ind. Eng. Chem. Res. **48**, 10021 (2009).

[184]G. Xomeritakis, S. Nair, and M. Tsapatsis, Microporous Mesoporous Mater. **38**, 61 (2000).

[185]B. Ilic and S. G. Wettstein, Microporous Mesoporous Mater. **239**, 221 (2017).

[186]G. W. Scherer, Transp. Porous Media **10**, 311–331 (2015).

[187]D. H. Moffat and K. E. Weale, Fuel **34**, 449 (1955).

[188]C. M. White, D. H. Smith, K. L. Jones, A. L. Goodman, S. A. Jikich, R. B. LaCount, S. B. DuBose, E. Ozdemir, B. I. Morsi, and K. T. Schroeder, Energy Fuels **19**, 659 (2005).

[189]T. A. Moore, Int. J. Coal Geol. **101**, 36 (2012).

[190]Z. Pan and L. D. Connell, Int. J. Coal Geol. **69**, 243 (2007).

[191]Z. Pan and L. D. Connell, Int. J. Coal Geol. **92**, 1 (2012).

[192]L. Brochard, M. Vandamme, R. J.-M. Pellenq, and T. Fen-Chong, Langmuir **28**, 2659 (2012).

[193]D. Espinoza, M. Vandamme, P. Dangla, J.-M. Pereira, and S. Vidal-Gilbert, J. Geophys. Res., B: Solid Earth **118**, 6113 (2013).

[194]D. N. Espinoza, M. Vandamme, J.-M. Pereira, P. Dangla, and S. Vidal-Gilbert, Int. J. Coal Geol. **134**, 80 (2014).

[195]J. Zhang, K. Liu, M. Clennell, D. Dewhurst, and M. Pervukhina, Fuel **160**, 309 (2015).

[196]D. N. Espinoza, M. Vandamme, P. Dangla, J.-M. Pereira, and S. Vidal-Gilbert, Int. J. Coal Geol. **162**, 158 (2016).

[197]R. Heller and M. Zoback, J. Unconv. Oil Gas Resour. **8**, 14 (2014).